Transforming Delayed Fluorescence to Blue-shifted Phosphorescence in Aminoboranes via Oxygen-to-Sulfur Exchange on Donor Amine.

Akkarakkaran Thayyil Muhammed Munthasir*, [a] Satyam Jena, [a] and Pakkirisamy Thilagar*[a]

[a] Department of Inorganic and Physical Chemistry, Indian Institute of Science, Bangalore-560012, India.

* Email: thilagar@iisc.ac.in

Table of Contents

1. General experimental procedures

1.1. Materials

The chemicals were purchased from commercial suppliers (Avra Scientific, India; Spectrochem, India; Merck, Germany) and used as received unless otherwise mentioned. The Standard Schlenk-line technique was used for reactions. THF was dried over sodium and distilled out under a nitrogen atmosphere.

1.2. Methods

^{1}H, ^{11}B, and ^{13}C NMR spectra were recorded at 25 °C on a Bruker Avance 400 MHz NMR Spectrometer operating at a frequency of 400 MHz for ^{1}H, 128 MHz for ^{11}B, and 100 MHz for ^{13}C. ^{1}H NMR spectra were referenced to TMS (0.00 ppm) as an internal standard. Chemical shift multiplicities are reported as singlet (s), doublet (d), triplet (t), quartet (q), and multiplet (m). 13C resonances were referenced to the $CDCl_3$ signal at ~77.67 ppm. ^{11}B NMR chemical shift values were referenced to the external standard boron signal of $BF_3{\cdot}Et_2O$. Electronic absorption spectra, fluorescence emission spectra, and time-resolved fluorescence (TRF) decay measurements were recorded on a SHIMADAZU UV-2600 spectrophotometer and FLS-980 EDINBURGH spectrometer, respectively. Time-gated emission spectra were recorded using the same FLS 980 fluorimeters by excitation source of a pulsed microsecond flash lamp (μF1) with a pulse width of 1.1 μs. Temperature-dependent emission studies were also performed using the same instrument with the help of an OXFORD cryostat. Solutions of all the compounds for spectral measurements were prepared using anhydrous spectrophotometric grade solvents and standard volumetric glassware. Quartz cuvettes with sealing screw caps were used for the solution state spectral measurements. Single crystal X-ray diffraction studies were carried out with a Bruker SMART APEX diffractometer at 90 K equipped with a 4-axis goniometer for all the compounds. The structures were solved by direct methods and refined by full-matrix least-squares on F2 using SHELXTL software. Density functional theory (DFT) calculations were done using B3LYP functional with 6-31G(d) basis sets as incorporated in the Gaussian 09 package for all the atoms.[1,2] The optimized structures and the frontier molecular orbitals (FMOs) were viewed using Gaussview 5.0. SOC calculations were done by ORCA 5.0 software, using B3LYP functional with B3LYP/G cc-pvdz basis sets and functional. All the ground state theoretical calculations are performed by using coordinates taken from the crystal structure after single-point energy calculation. Output coordinates from this calculation are further taken for excited state calculations.

2. Synthesis

2.1 Synthesis of BNO and BNS

General procedure

BNO and **BNS** are synthesized according to the reported literature procedure.[3] A hexane solution of n-BuLi (1.6 M, 1.1eq) was added dropwise to anhydrous THF solution of 10*H*-phenothiazine or 10*H*-phenoxazine (1 eq) at around -78 °C under continuous stirring. A solution of bis(2,6-dimethylphenyl)fluoroborane (1.2 eq) in anhydrous THF was added to the reaction mixture after 1.5 h at -78 ℃. The reaction mixture was allowed to warm to room temperature, and the stirring was continued for another 12 h. After the completion of the reaction, volatile organic solvents were removed under reduced pressure. The resultant residue was dissolved in dichloromethane and washed with water (3x100 mL). DCM layer was dried over Na_2SO_4 and the removal of organic volatiles under reduced pressure afforded crude product. Analytically pure compound was obtained by column chromatography over silica gel and further recrystallization from Hexane: DCM mixture (1:3) (for **BNO**) or DCM (for **BNS**) by slow evaporation.

Synthesis of 10-(bis(2,6-dimethylphenyl)boraneyl)-10H-phenoxazine (BNO)[3.a]

Compound **BNO** was synthesized following the general procedure depicted above **BNS**. The reagents involved, the quantity used, and the characterization data are as follows. Hexane solution of n-BuLi (1.6 M, 8.2 ml), 10*H*-phenoxazine (2.0 g, 10.92 mmol) and bis(2,6-dimethylphenyl)fluoroborane (2.9 g, 12.0 mmol) in anhydrous THF. The analytically pure product was obtained after silica gel column chromatography using DCM: hexane (v/v=1/9) as eluent and recrystallization from Hexane: DCM mixture in the 1:3 ratio. Pale yellow crystals (**BNO**), Yield: 2.9 g (65 %), ^{1}H NMR (400 MHz, $CDCl_3$, 25 °C) δ (ppm) 7.08 (t, *J* = 8.0 Hz, 2H), 7.01 (dd, *J* = 8.0 Hz, 4.0 Hz 2H), 6.97 (t,d *J* = 8.0 Hz, 4.0 Hz 2H),6.87 (t, *J* = 8.0 Hz, 6H), 6.6 (t, *J* = 8.0 Hz, 2H), 2.31 (s, 12H). ^{11}B NMR (160 MHz, $CDCl_3$, 25 °C) δ (ppm): 50.7. ^{13}C NMR (125 MHz, $CDCl_3$, 25 °C) δ (ppm) 149.7, 141.8, 140.9, 133.7, 128.3, 127.2, 125.3, 123.1, 122.6, 116.4, 22.5. HRMS (m/z)- $C_{28}H_{26}BNOH$ - calculated: 404.2185 (M+H), found:404.2183.

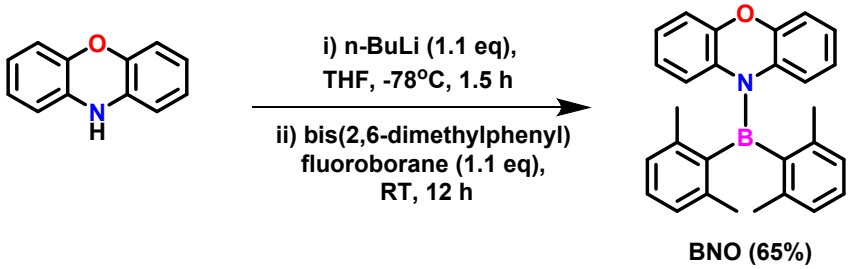

Scheme S1. Synthesis of **BNO.**

Synthesis of 10-(bis(2,6-dimethylphenyl)boraneyl)-10H-phenothiazine (BNS)[3.b]

Compound **BNS** was synthesized following the general procedure depicted above. The reagents involved, the quantity used, and the characterization data are as follows. Hexane solution of n-BuLi (1.6 M, 7.53 ml), 10H-phenothiazine (2g, 10.04 mmol) and bis(2,6-dimethylphenyl)fluoroborane (2.65 g 11.04 mmol) in anhydrous THF. The analytical pure product is obtained by silica column chromatography using hexane as eluent and recrystallization from the DCM solution. The product 10-(bis(2,6-dimethylphenyl)boraneyl)-10H-phenothiazine obtained as colourless crystals. Yield: 3.45 g (82 %). ^{1}H NMR (400 MHz, $CDCl_3$, 25 °C): δ (ppm) 7.26-7.29 (d, *J* = 8 Hz, 2H), 7.15-7.18 (d *J* = 8.0 Hz, 2H), 7.02-7.05 (m, 2H) 6.98-7.01 (m, 2H), 6.84-6.90 (m, 6H), 2.45 (s, 12H). ^{11}B NMR (160 MHz, $CDCl_3$, 25 °C) δ (ppm): 50.20. ^{13}C NMR (125 MHz, $CDCl_3$, 25 °C) δ (ppm) 143.1, 141.4, 140.6, 129.8,127.7,127.1, 127.0,126.3, 125.3,125.2,24.2. HRMS (m/z)- $C_{28}H_{26}BNS$- calculated: 419.1875 (M+), found: 419.1880

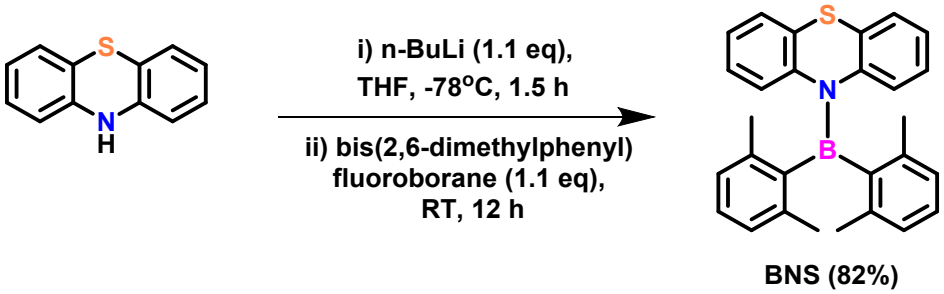

Scheme S2. Synthesis of **BNS**.

3. Structural charecterization

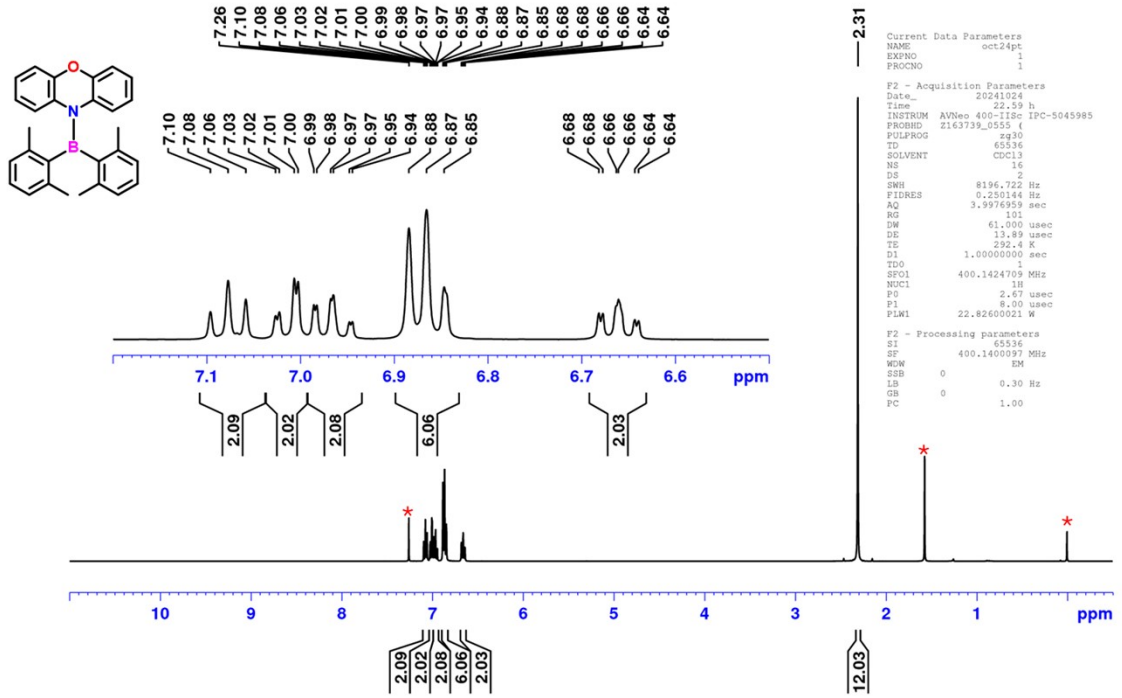

Figure S1. ^{1}H NMR spectrum of **BNO** in $CDCl_3$ at 25°C. [Peaks marked with an asterisk are residual solvent peaks $CDCl_3$ (δppm = 7.26), H_2O (δppm= 1.55) and TMSCl (δppm= 0.00)]

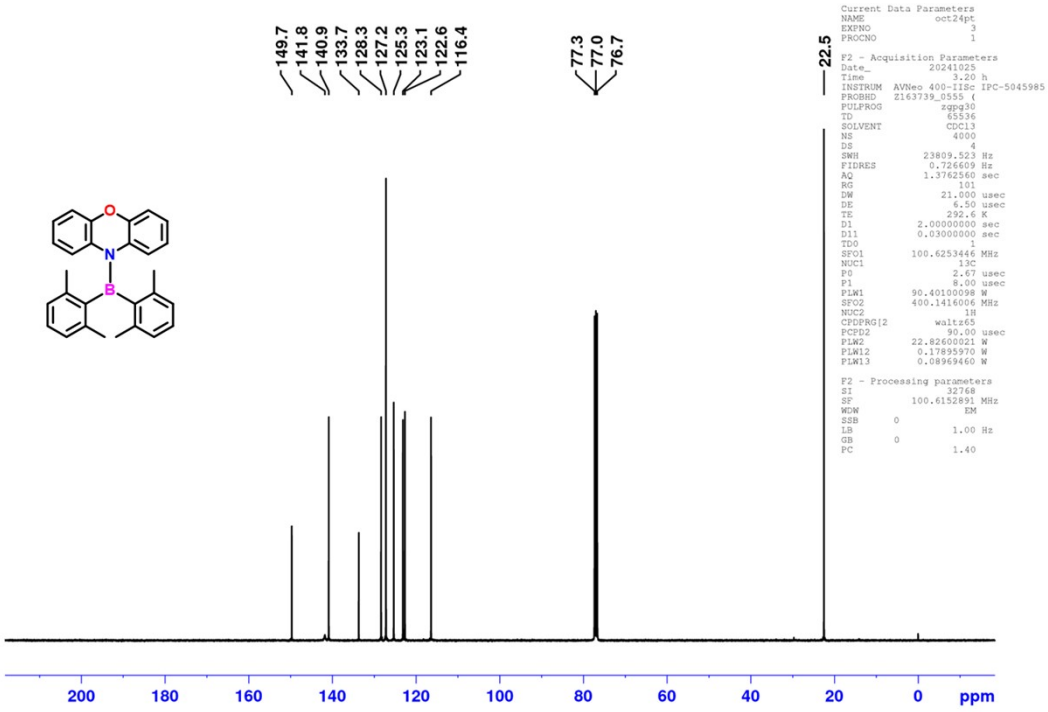

Figure S2. ^{13}C NMR spectrum of **BNO** in $CDCl_3$ at 25°C.

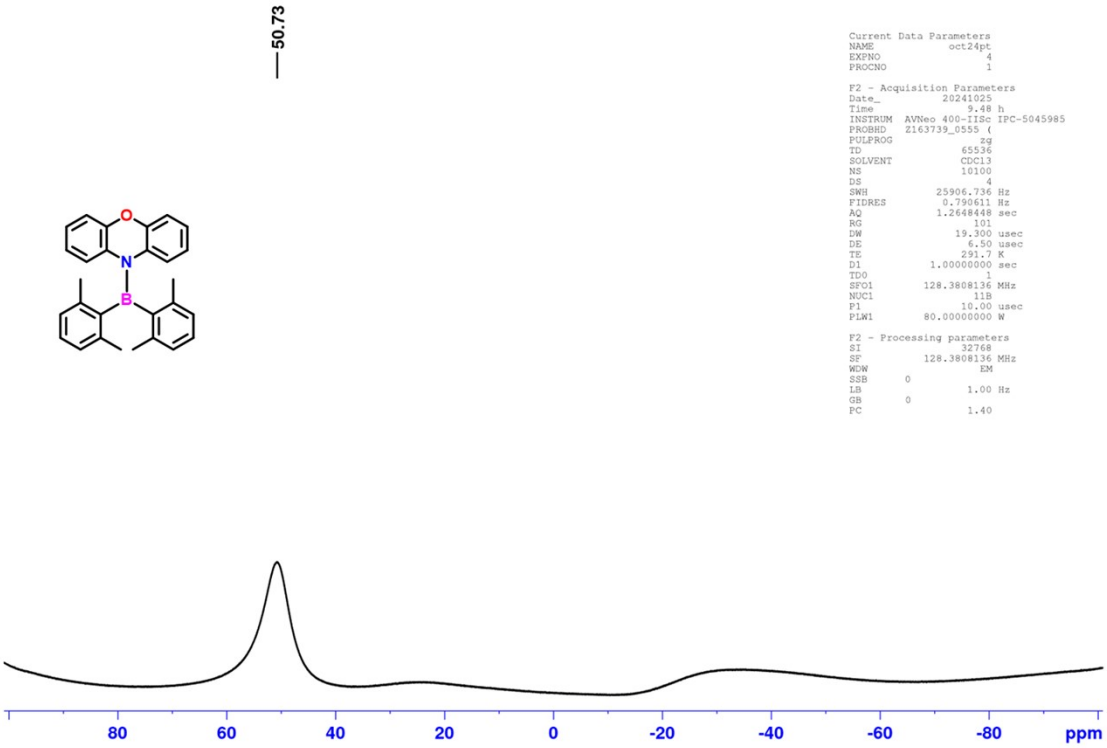

Figure S3. ^{11}B NMR spectrum of **BNO** in $CDCl_3$ at 25°C.

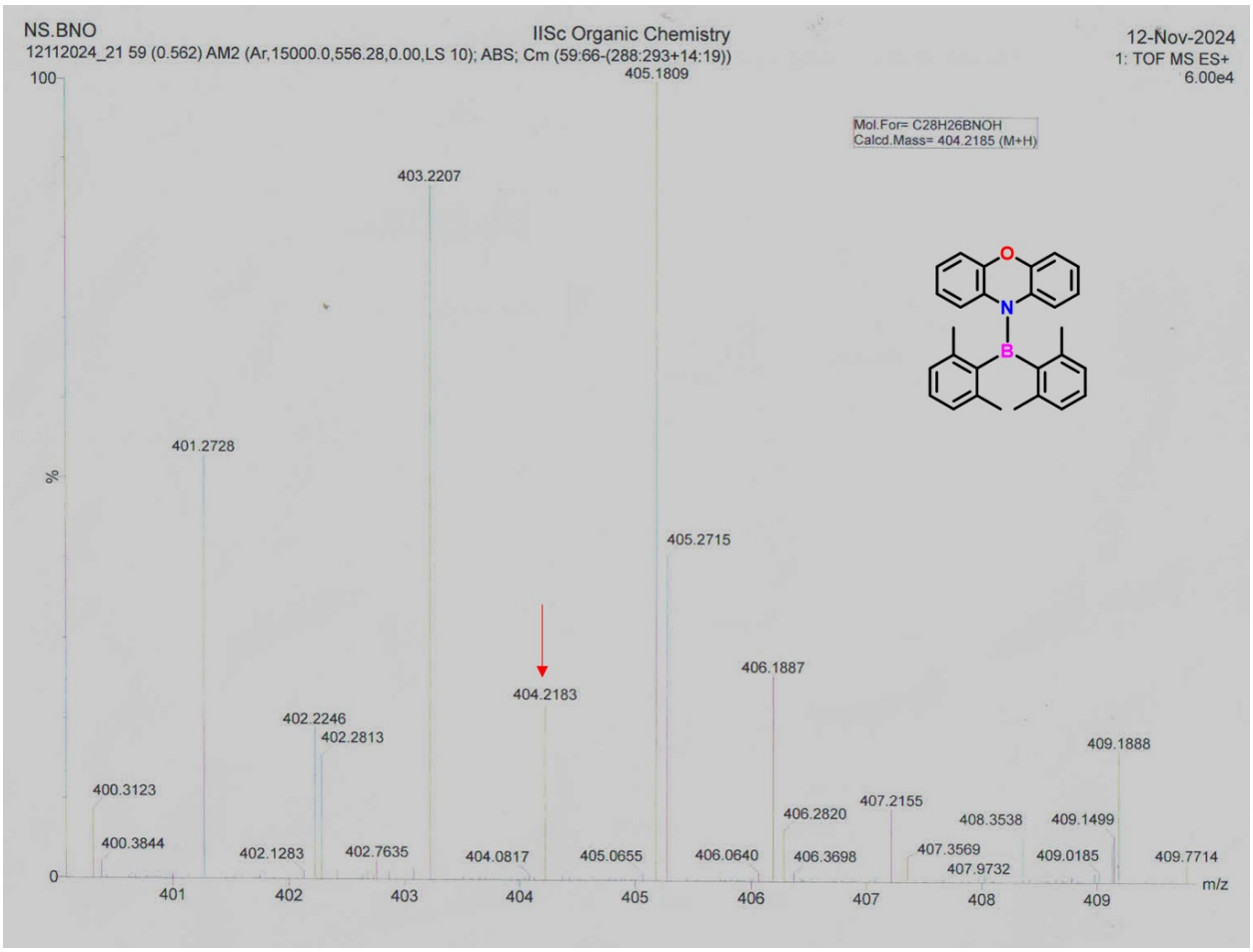

Figure S4. High-resolution mass (HRMS) spectrum of **BNO.**

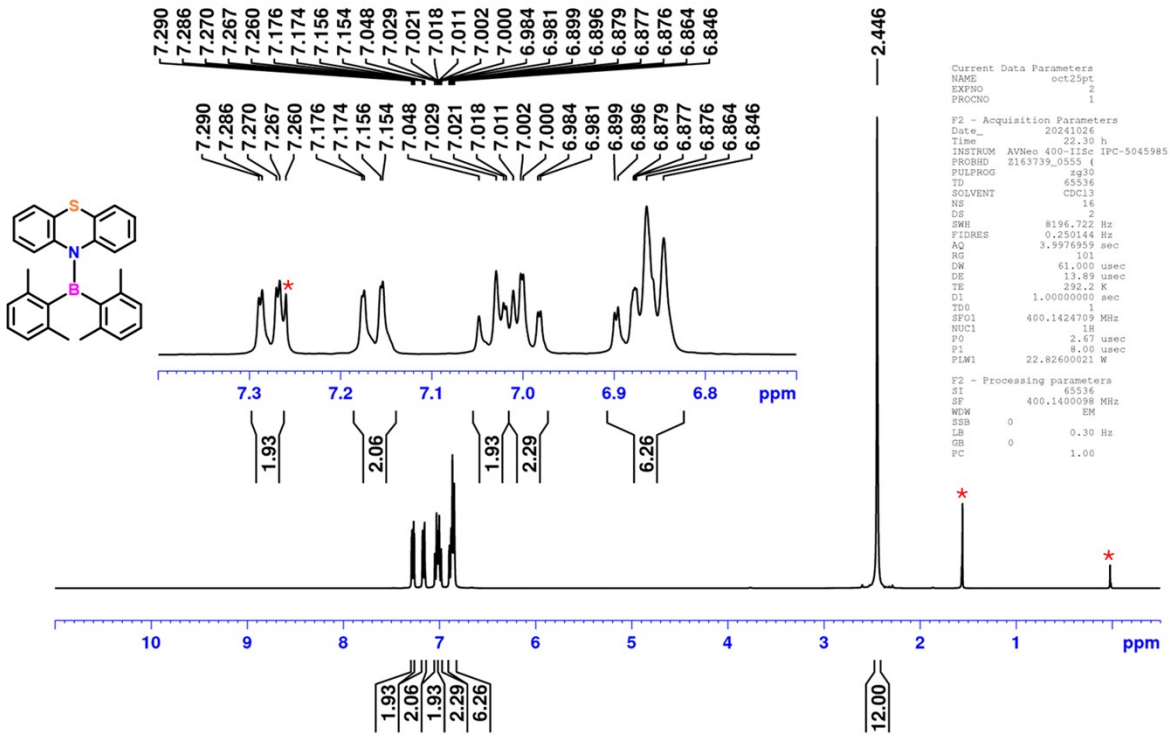

Figure S5. ^{1}H NMR spectrum of **BNS** in $CDCl_3$ at 25°C. [Peaks marked with an asterisk are residual solvent peaks $CDCl_3$ (δppm = 7.26), H_2O (δppm= 1.55) and TMSCl (δppm= 0.00)]

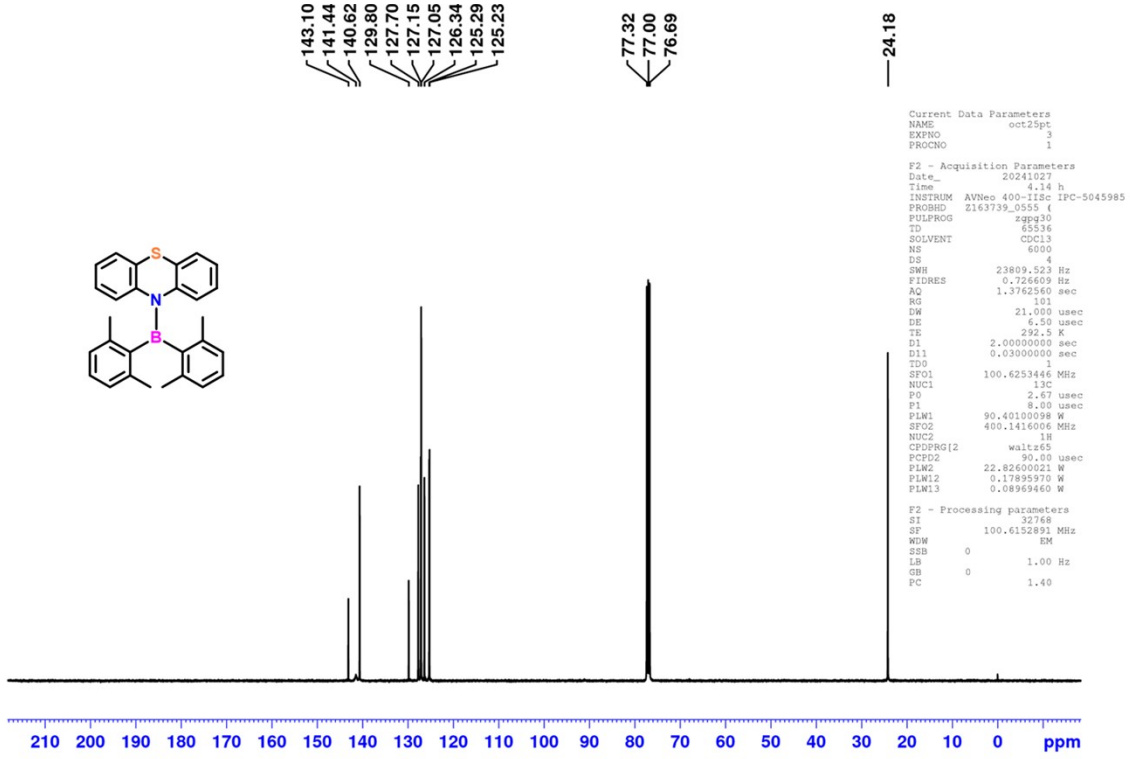

Figure S6. ^{13}C NMR spectrum of **BNS** in $CDCl_3$.at 25°C.

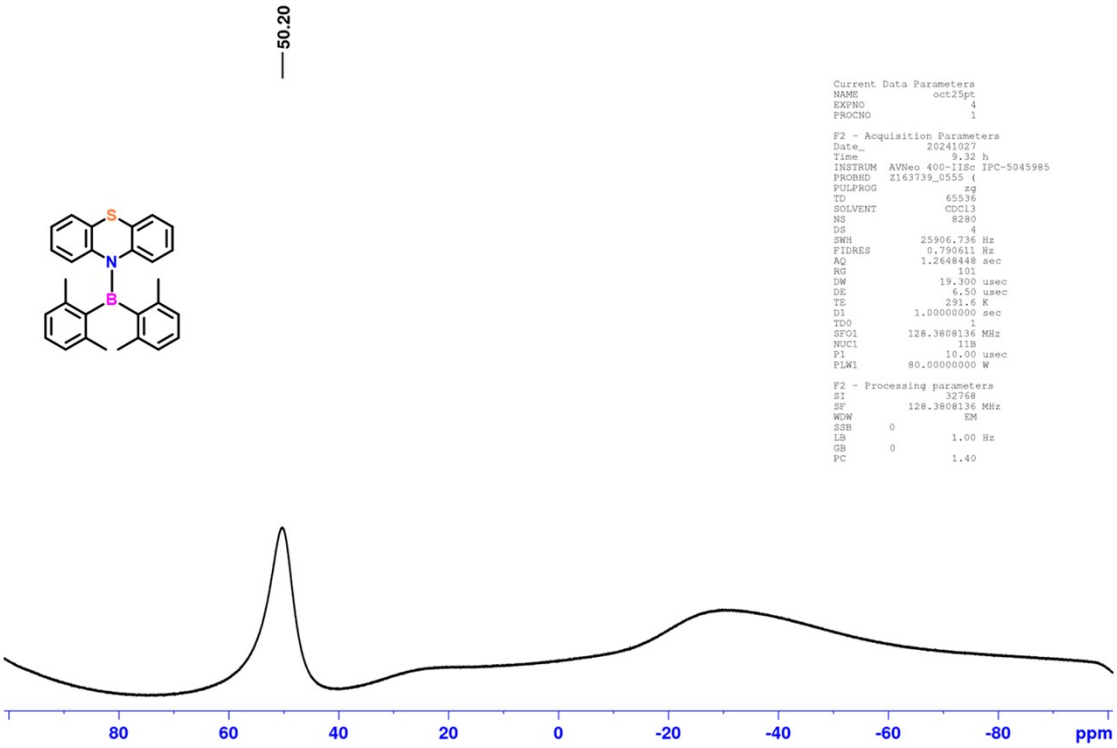

Figure S7. ^{11}B NMR spectrum of **BNS** in $CDCl_3$ at 25°C.

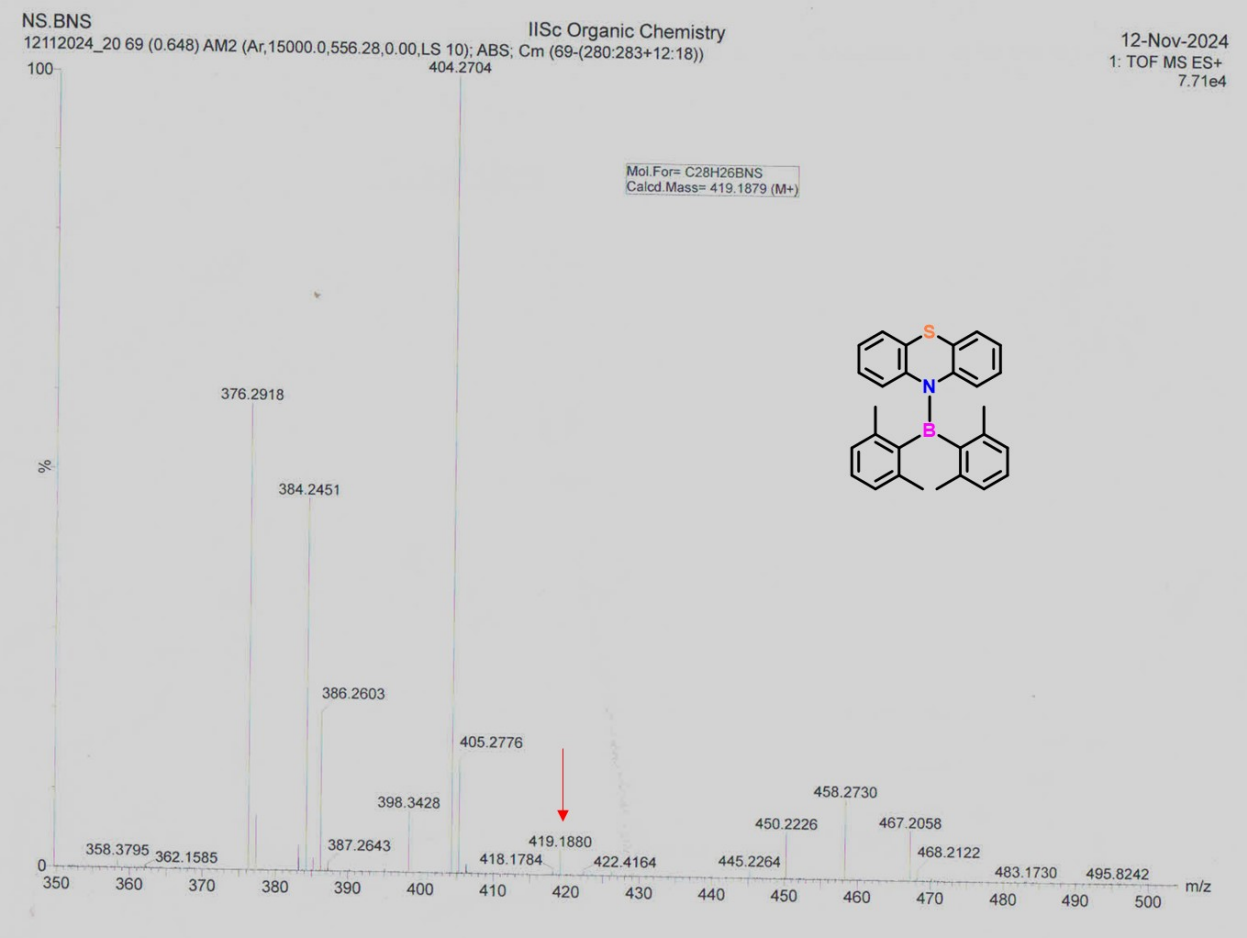

Figure S8. High-resolution mass (HRMS) spectrum of **BNS**

4. Crystal data.

Table S1: Crystallographic data and refinement parameters for **BNO.**

Compound	**BNO**
Empirical formula	C_{28} H_{26} B N O
FW	403.31
T (K)	100(2) K
Crystal system	Triclinic
Space group	*P -1*
a/Å	9.6034(2)
b/Å	10.4382(3)
c/Å	12.1561(3)
α/deg	101.682(1)
β/deg	103.810(1)
γ/deg	104.221(1)
V/Å^3	1102.05(5)
Z	2
ρ_{calcd} (gcm^{-3})	1.215
μ (Mo Kα) (mm^{-1})	0.069
λ/Å	0.71073
F (000)	428
Collected reflections	6646
Unique reflections	5131
GOF (F2)	1.066
R1 [I>2σ(I)][a]	0.0563
wR2 [I>2σ(I)][b]	0.1897
CCDC Number	2402292

[a] R1 = Σ||Fo| − |Fc||/ Σ|Fo|. [b] wR2 = [Σ{w(Fo 2 – Fc 2) 2 }/Σ{w(Fo 2)

Table S2: The selected bond lengths and dihedral angles between different aromatic rings were measured from crystal structures of **BNO** and **BNS .**[3.b]

Compound	B-N bond length (Å)	Dihedral angle (deg)	The angle between the xylyl plane(deg)	The angle between the phenyl plane in phenoxazine/phenothiazine (deg)
BNO	1.433	28.70	86.80	146.35
BNS	1.445	22.31	82.73	134.08

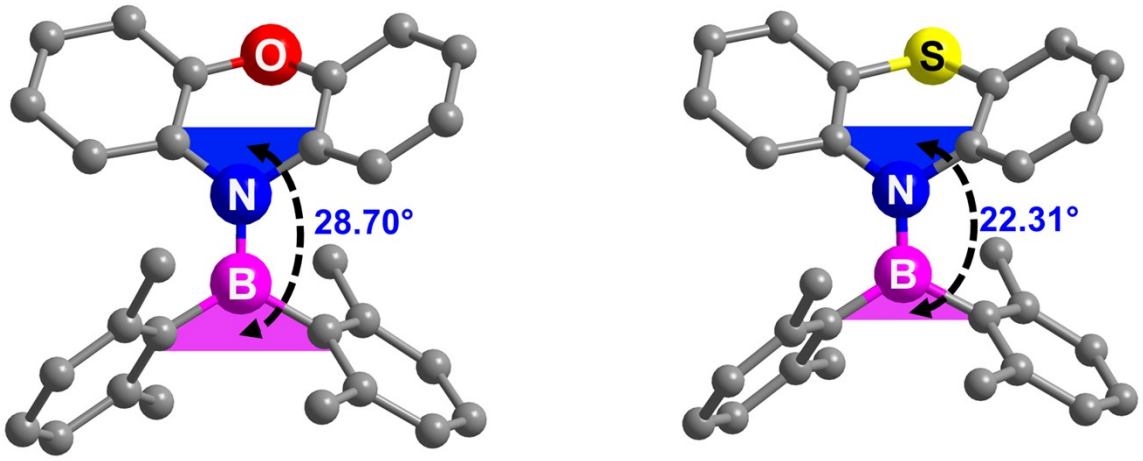

Figure S9. Dihedral angle (deg) between the plane containing a nitrogen atom and carbon directly attached to it (CNC) in phenoxazine/phenothiazine (blue) and the plane containing a boron atom and carbon atoms directly attached to it (CBC) in bisarylborane (magenta). The angles between the planes were calculated from crystal structures using mercury software.

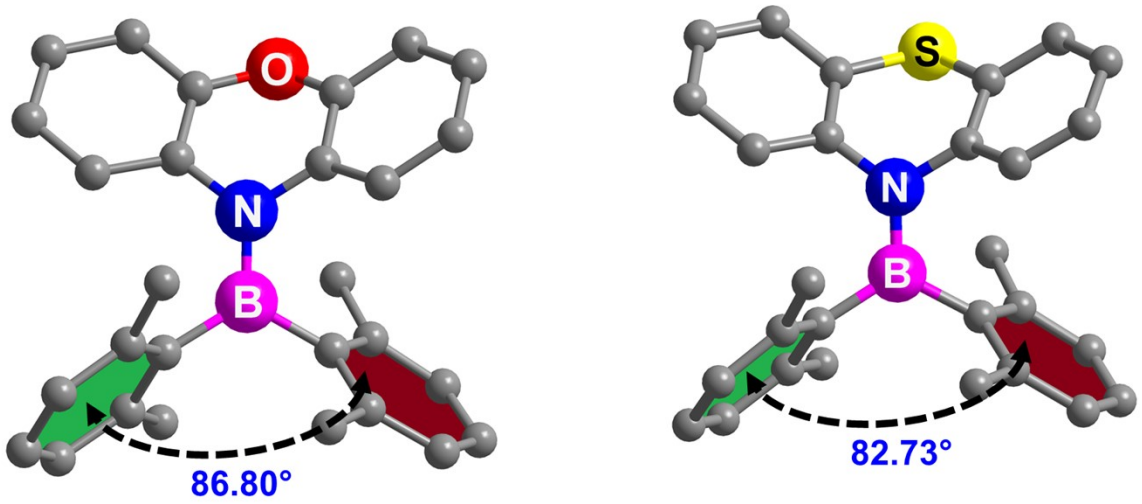

Figure S10. Angle (deg) between two aryl planes attached to the boron in **BNO** and **BNS.** The angles between the planes were calculated from crystal structures using mercury software.

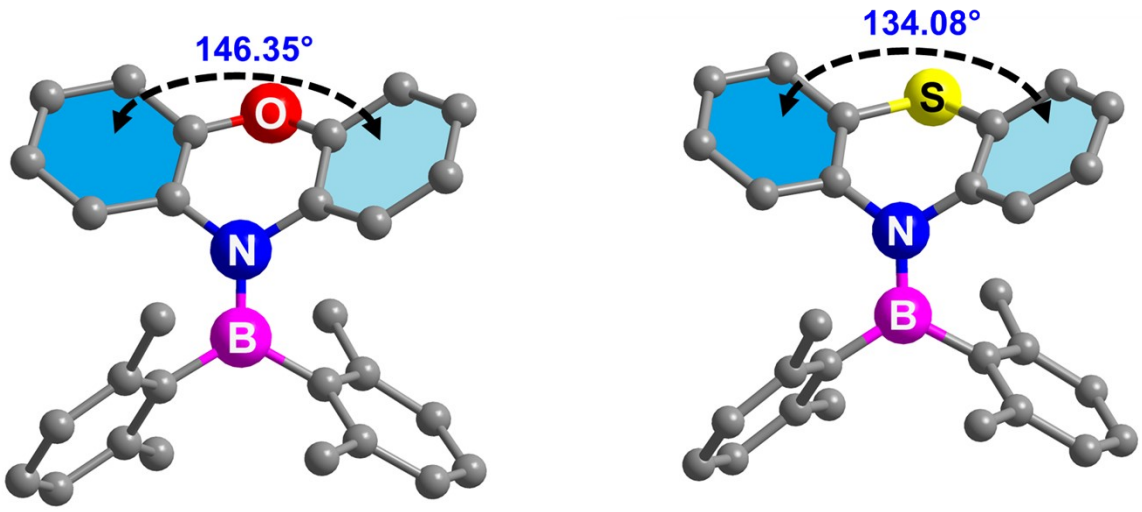

Figure S11. Puckering angle (°) in (a) phenoxazine of **BNO** and (b) phenothiazine of **BNS.** The angles between the planes were calculated from crystal structures using mercury software.

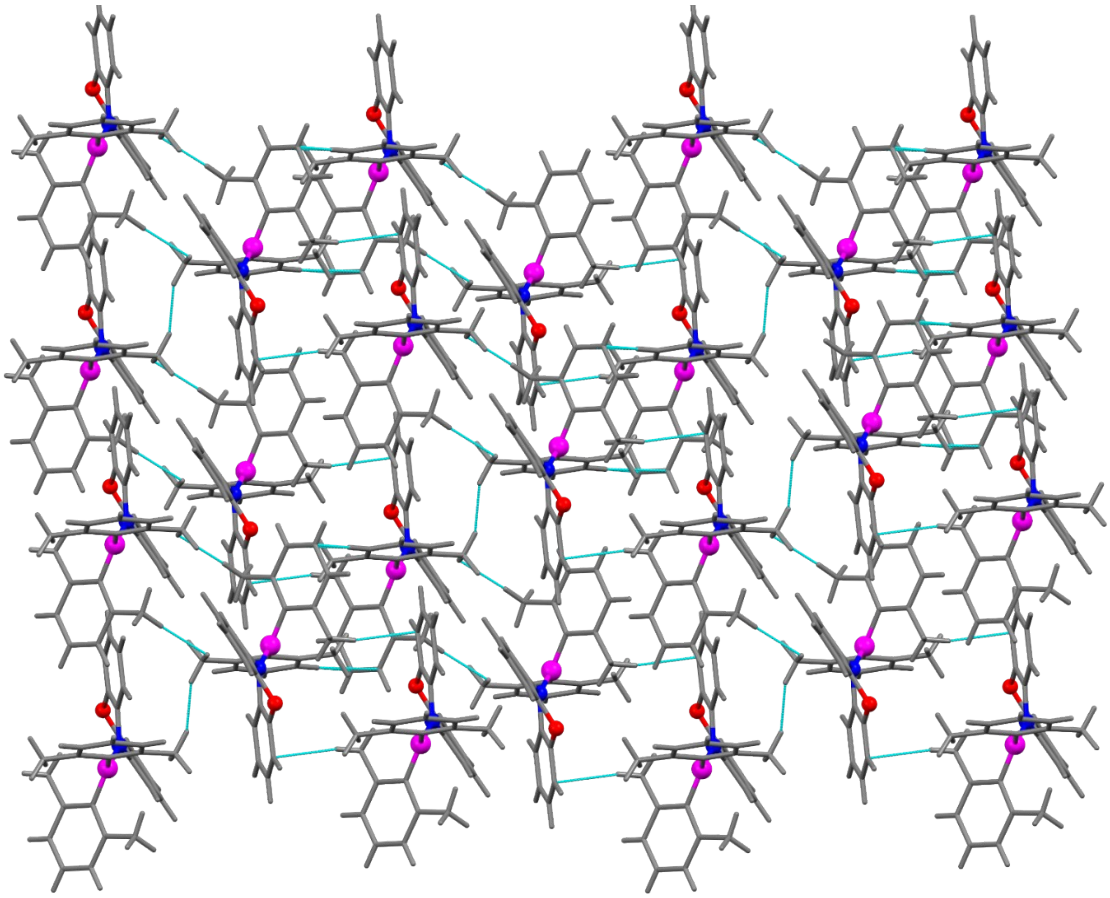

Figure S12: 3D supramolecular structure of **BNO** [cyan dashed line represents the CH---π interactions (2.849Å and 3.31Å), atom color code: carbon: grey, nitrogen: blue, oxygen: red and hydrogen off white]

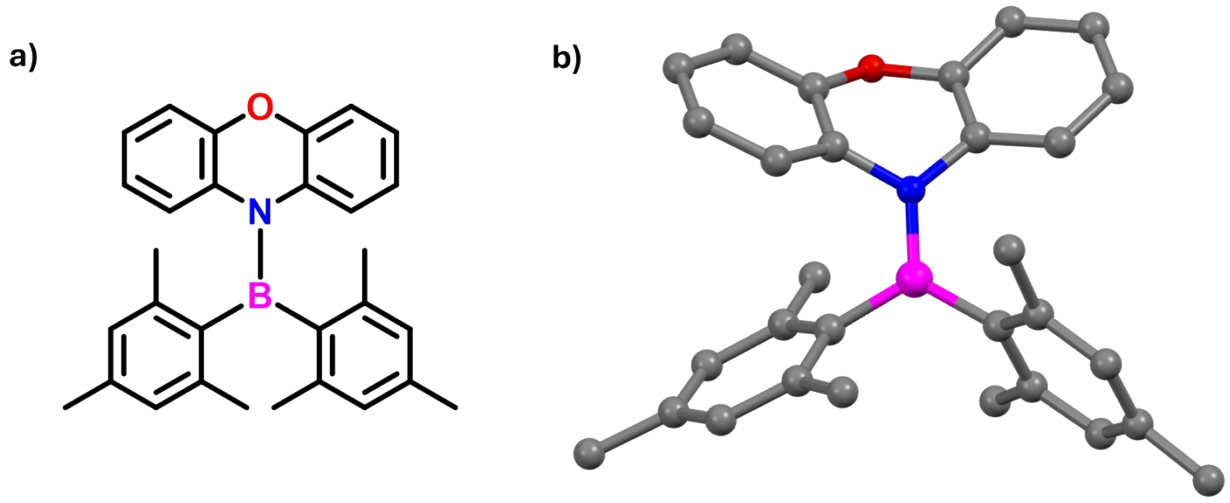

Figure S13. (a) Chemical and (b) molecular structure of **R1**[3.a].

5. Photophysical and Theoretical Data

5.1 Solution-state photoluminescence

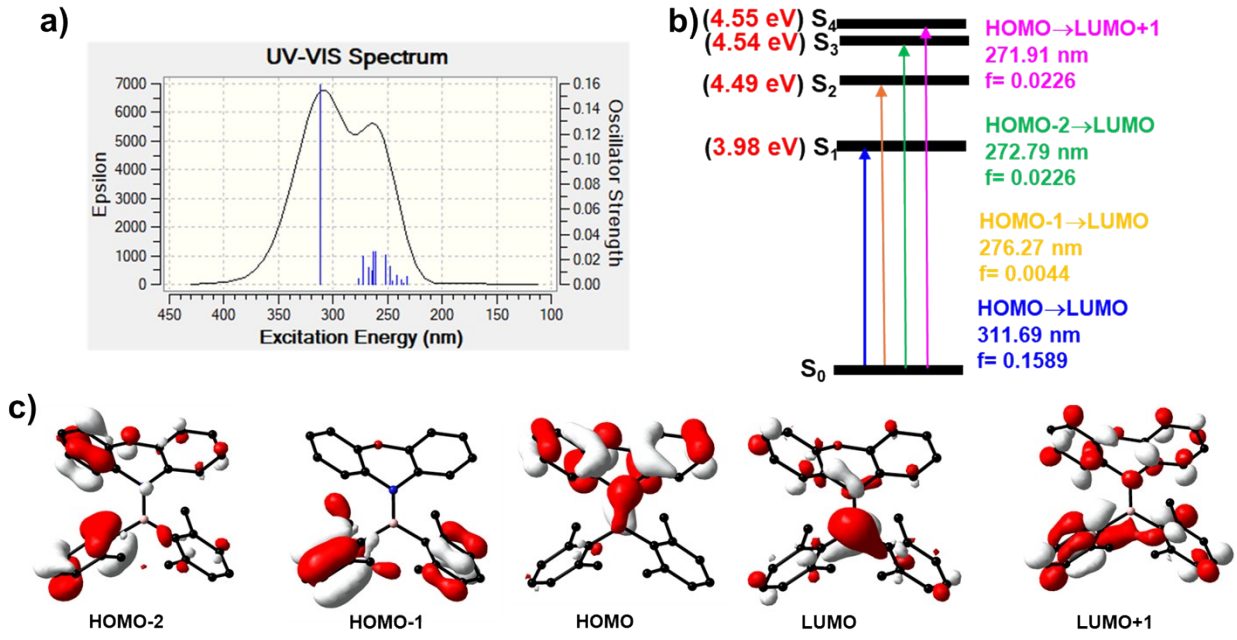

Figure S14. (a) Simulated UV-visible absorption spectra and (b) corresponding singlet vertical transition computed from TD-DFT calculations. (c) Molecular orbitals involved in the transitions are obtained from optimized ground state geometries of **BNO** using DFT at B3LYP and 6-31G (d) level of theory**.**

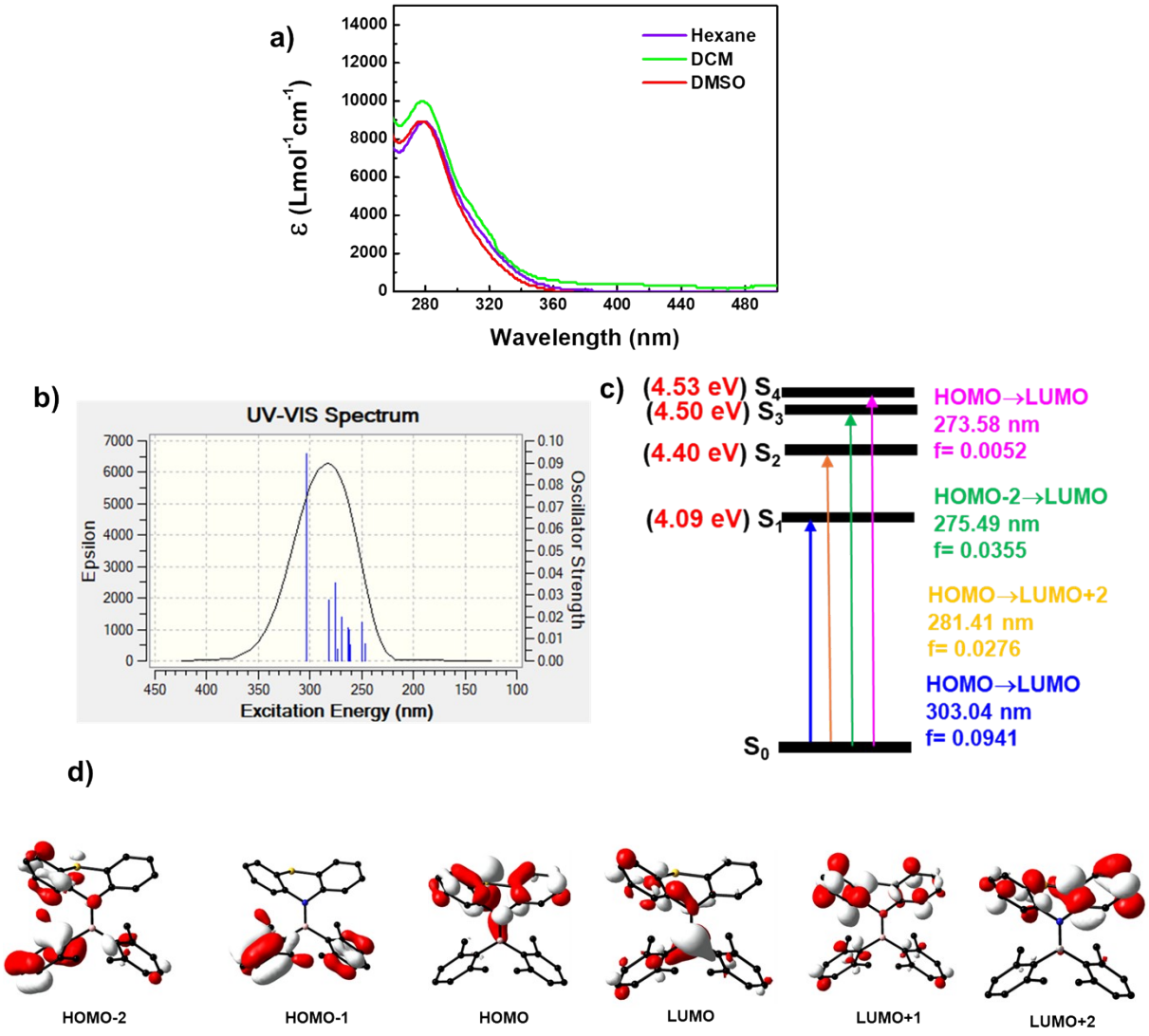

Figure S15. (a) UV-visible absorption spectra of BNS in different solvents (conc. 10^{-5} M). (b) Simulated UV-visible absorption spectra and (c) corresponding singlet vertical transition computed from TD-DFT calculations. (d) Molecular orbitals involved in the transitions are obtained from optimized ground state geometries of **BNO** using DFT at B3LYP and 6-31G-(d) level of theory**.**

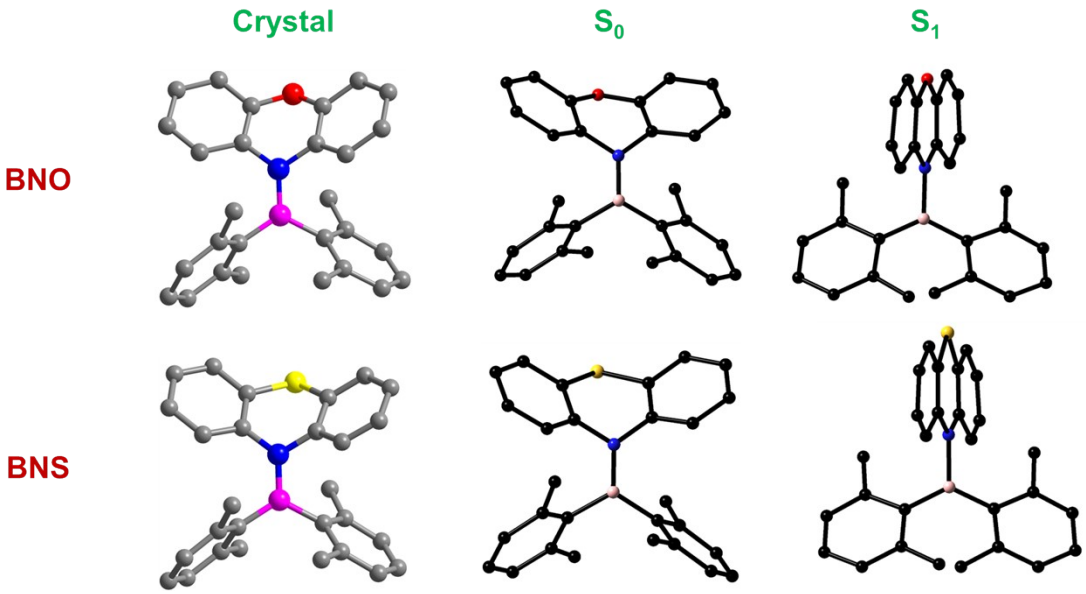

Figure S16. Molecular structure and ground state (S_0) and first singlet excited state optimized geometry (S_1) for **BNO** and **BNS.** Computation details: DFT/TD-DFT at B3LYP and 6-31G (d) level of theory.

Table S3. The selected bond parameters for **BNS** and **BNO were** obtained from the crystal structure and S_0 and S_1 optimized geometry. Computation details: DFT/TD-DFT at B3LYP and 6-31G (d) level of theory.

Compound	B-N bond length (Å)	BC bond length (Å)	Dihedral angle (Θ_{BN}) (deg)	The angle between the xylyl plane (Θ_{xy}) (°)	The angle between the phenyl plane in phenoxazine/phenothiazine (Θ_{xy}/ (Θ_{xy}) (°)
	Crystal				
BNO	1.433	1.590 1.583	28.70	86.80	146.35
BNS	1.445	1.603 1.591	22.31	82.73	134.08
	Ground state-optimized geometry (S_0)				
BNO	1.434	1.594 1.600	23.92	84.59	146.59
BNS	1.446	1.608 1.608	18.96	81.51	135.86
	Excited state-optimized geometry (S_1)				
BNO	1.619	1.552 1.552	69.42	72.01	174.51
BNS	1.630	1.554 1.554	68.94	70.15	172.92

Table S4. Summary of TD-DFT computed singlet vertical transitions involved in **BNO**.

Transitions	E/eV	λ/nm	f	Dominant transitions (%)
$S_0 \rightarrow S_1$	3.9778	311.69	0.1589	HOMO →LUMO (48.70)
$S_0 \rightarrow S_2$	4.4877	276.27	0.0044	HOMO-1 →LUMO (45.46)
$S_0 \rightarrow S_3$	4.5450	272.79	0.0226	HOMO-2 →LUMO (41.40)
$S_0 \rightarrow S_4$	4.5597	271.91	0.0055	HOMO →LUMO +1 (21.28) HOMO →LUMO +2 (24.20)
$S_0 \rightarrow S_5$	4.6432	267.02	0.0138	HOMO →LUMO+1 (21.53)
$S_0 \rightarrow S_6$	4.7101	263.23	0.0263	HOMO-4 →LUMO (27.52) HOMO-3 →LUMO (8.23)
$S_0 \rightarrow S_7$	4.7515	260.94	0.0259	HOMO →LUMO+3 (34.57) HOMO-5 →LUMO+2 (1.60)

Table S5. Summary of TD-DFT computed singlet vertical transitions involved in **BNS**.

Transitions	E/eV	λ/nm	f	Dominant transitions (%)
$S_0 \rightarrow S_1$	4.0913	303.04	0.0941	HOMO →LUMO (47.76)
$S_0 \rightarrow S_2$	4.4058	281.41	0.0276	HOMO →LUMO+2 (34.79) HOMO →LUMO+1 (12.15)
$S_0 \rightarrow S_3$	4.5006	275.49	0.0355	HOMO →LUMO+1 (17.44) HOMO-2 →LUMO (17.45)
$S_0 \rightarrow S_4$	4.5320	273.58	0.0052	HOMO →LUMO (44.81)
$S_0 \rightarrow S_5$	4.6008	269.49	0.0200	HOMO-2→LUMO (25.76)
$S_0 \rightarrow S_6$	4.7115	263.15	0.0152	HOMO →LUMO+3 (36.5)
$S_0 \rightarrow S_7$	4.7248	262.41	0.0140	HOMO-4 →LUMO (40.45)

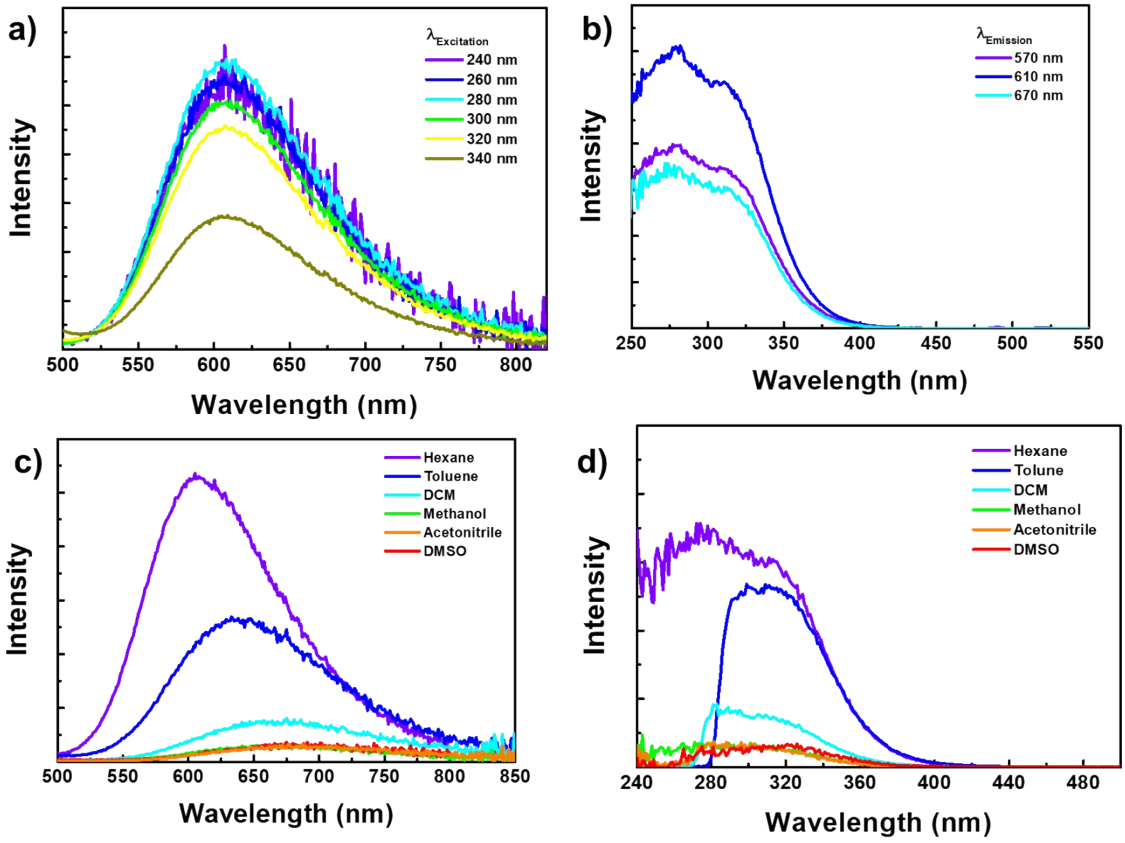

Figure S17. (a) **E**xcitations-dependent photoluminescence [PL] and (b) emission-dependent excitation spectra for **BNO** in hexane (conc. 10^{-5} M). (c) Steady-state PL spectra and (d) corresponding excitation spectra for **BNO** in different solvents (conc. 10^{-5} M) at λ_{ex}= 310 nm.

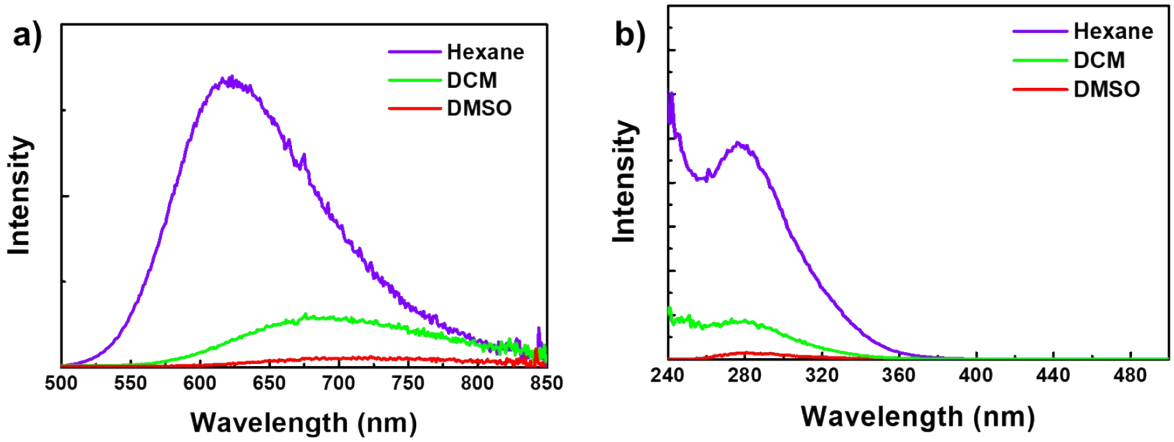

Figure S18. (a) steady-state PL spectra (b) corresponding excitation spectra for **BNS** in different solvents (conc. 10^{-5} M) at λ_{ex}= 310 nm.

Table S6. Selected photophysical data for **BNO** and **BNS** in different solvents (conc. 10^{-5} M) .(nd: Not detectable)

	Solvent	λ_{abs} [nm] **(ϵ)** [mol^{-1} L cm^{-1}]	λ_{em} [nm]	PL lifetime [ns] λ_{ex} **= 300 nm** τ_1 (A_1)	**PLQY** [%]
BNO	Hexane	282 (7245) 315 (5581)	605	11.78 (100)	8.0 %
	Toluene	282 (-) 315 (5581)	635	nd	nd
	DCM	281 (10433) 312 (7940))	665	nd	nd
	Methanol	282 (5636) 314 (4389)	668	nd	nd
	Acetonitrile	281 (6476) 310 (5029)	687	nd	nd
	DMSO	282 (7245) 315 (5581)	687	nd	nd
BNS	Hexane	278 nm (8904)	620	11.18 (100)	nd
	DCM	278 nm (10025)	680	nd	nd
	DMSO	278 nm (8905)	685	nd	nd

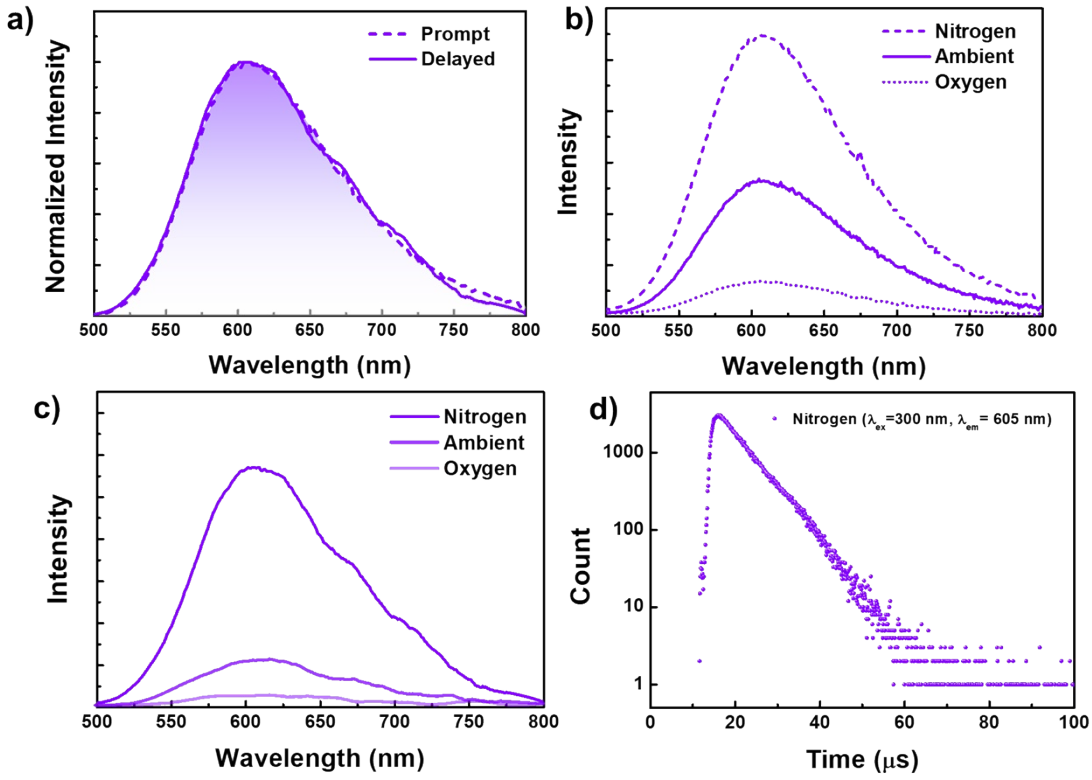

Figure S19. (a) Prompt and time-gated/delayed [10μs delay] PL spectra (λ_{ex} = 310 nm) for **BNO** in hexane purged with nitrogen gas. (b) Steady-state PL spectra and (c) time-gated/delayed [20μs delay] PL spectra (λ_{ex} = 310 nm) for **BNO** in hexane under different environments. (d) delayed fluorescence decay fit for **BNO** in hexane, purged with nitrogen gas (λ_{ex} = 310 nm, λ_{em} = 605 nm, and conc. 10^{-5} M.

Table S7. Fluorescence (Fl), delayed fluorescence (DF) lifetime, and total photoluminescence quantum yield for **BNO** in Hexane (conc. 10^{-5} M) under different environments (nd : Not detectable).

Atmosphere		λ_{ex} (nm)	λ_{em} (nm)	τ_1 (A_1)	PLQY
N_2	Fl	310	605	13.60 ns (100)	0.12
	DF	310	605	6.38 μs (100)	
Ambient	Fl	330	605	11.78 ns (100)	0.08
	DF	nd			
O_2	Fl	330	605	10.20 ns (100)	0.01
	DF	nd			

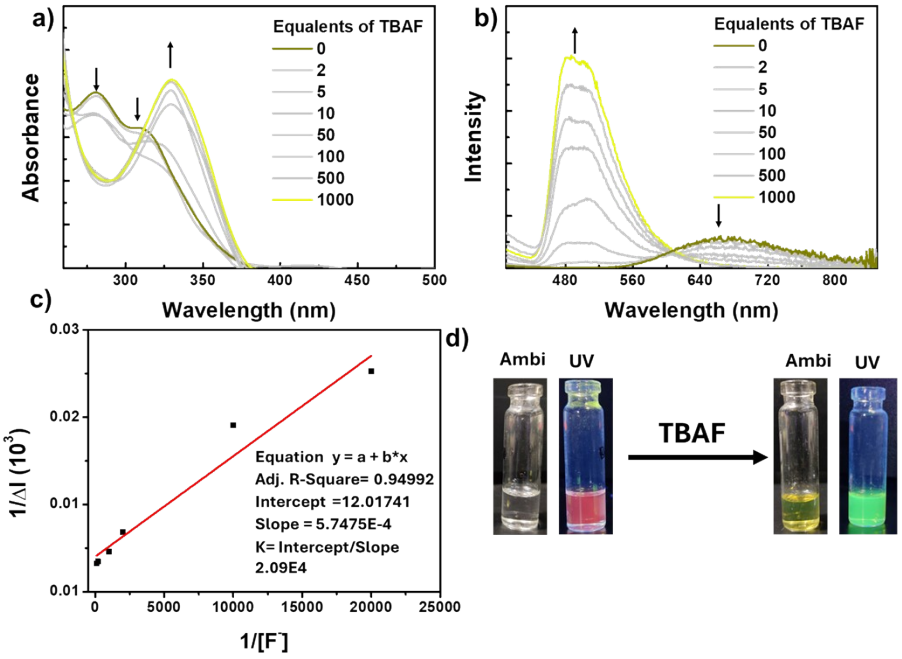

Figure S20. Change associated with (a) UV-visible absorption (b) steady-state PL spectra of **BNO** in DCM (Con 10^{-5} M) against different concentrations of tetrabutylammonium fluoride (1M TBAF in DCM). (c) Benesi-Hilderbrand plot for **BNO**: 1/ΔI = A + B/[F-], K = A/B. (d) Digital photographs of DCM solution of **BNO** with and without TBAF. [K is the binding constant].

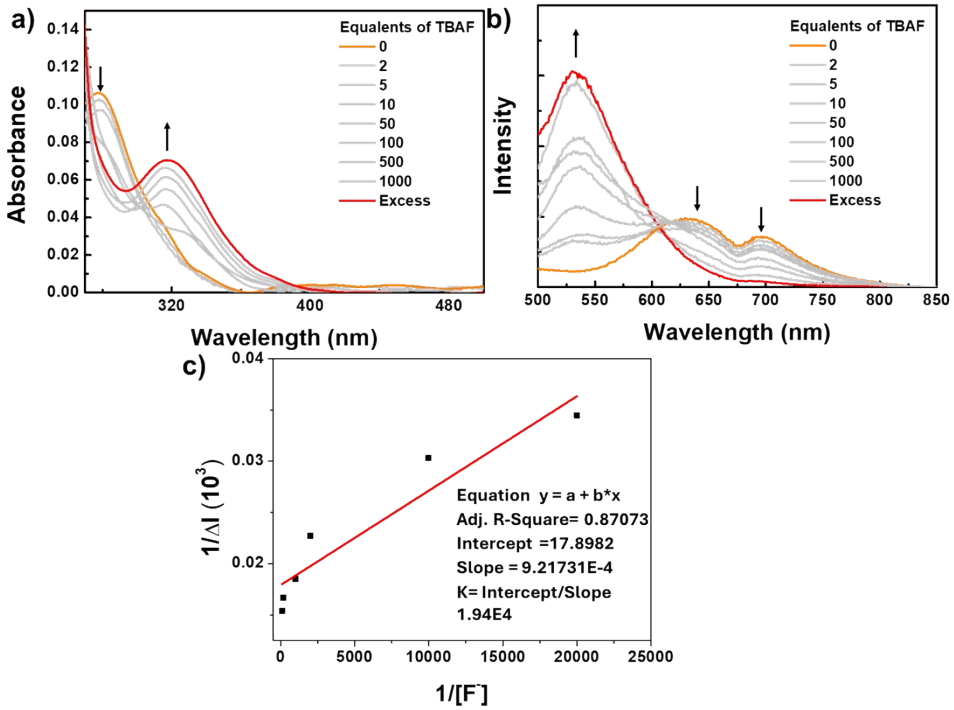

Figure S21. Changes associated with (a) UV-visible absorption (b) steady-state PL spectra of **BNS** in DCM (Con 10^{-5} M) against different concentrations of tetrabutylammonium fluoride (1M TBAF in DCM). (c) Benesi-Hilderbrand plot for **BNS**: 1/ΔI = A + B/[F-], K = A/B. (d) [K is the binding constant].

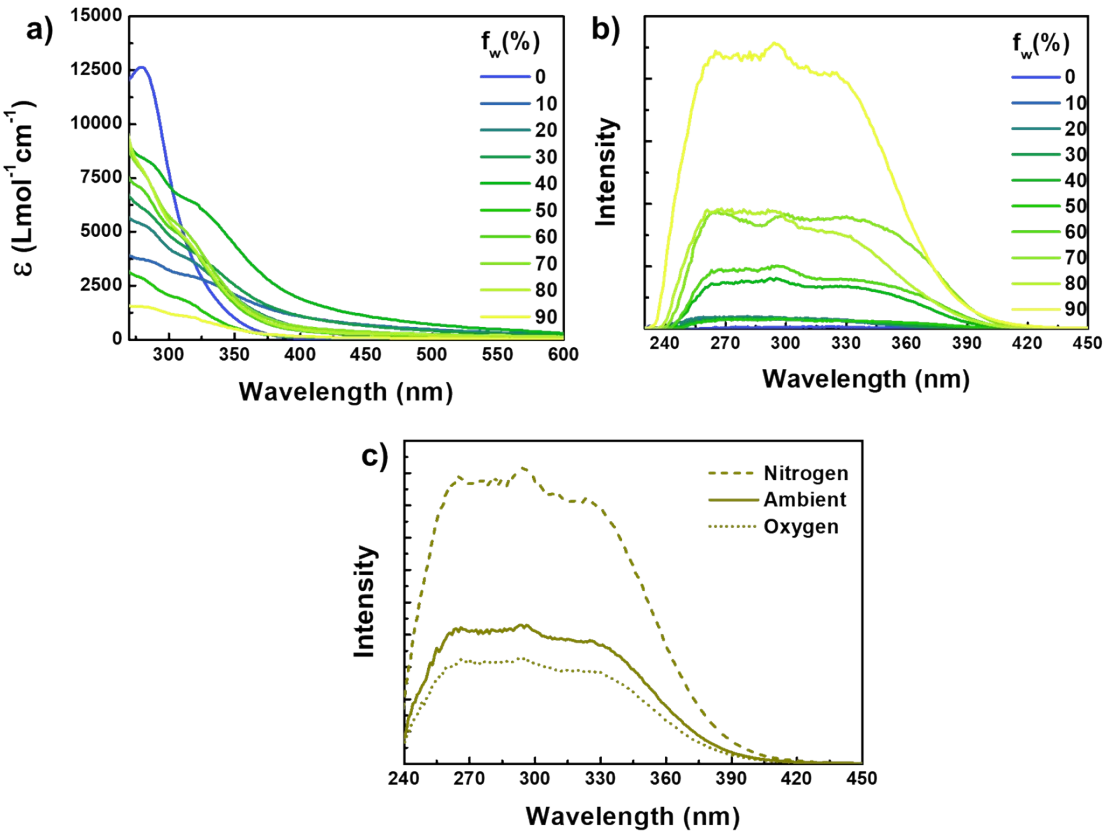

Figure S22. (a) Absorption and (b) excitation spectra of **BNO** in DMSO with different water fractions [f_w]. (c) excitation spectra for **BNO** in DMSO-water mixture, f_w = 90%, under different environments.

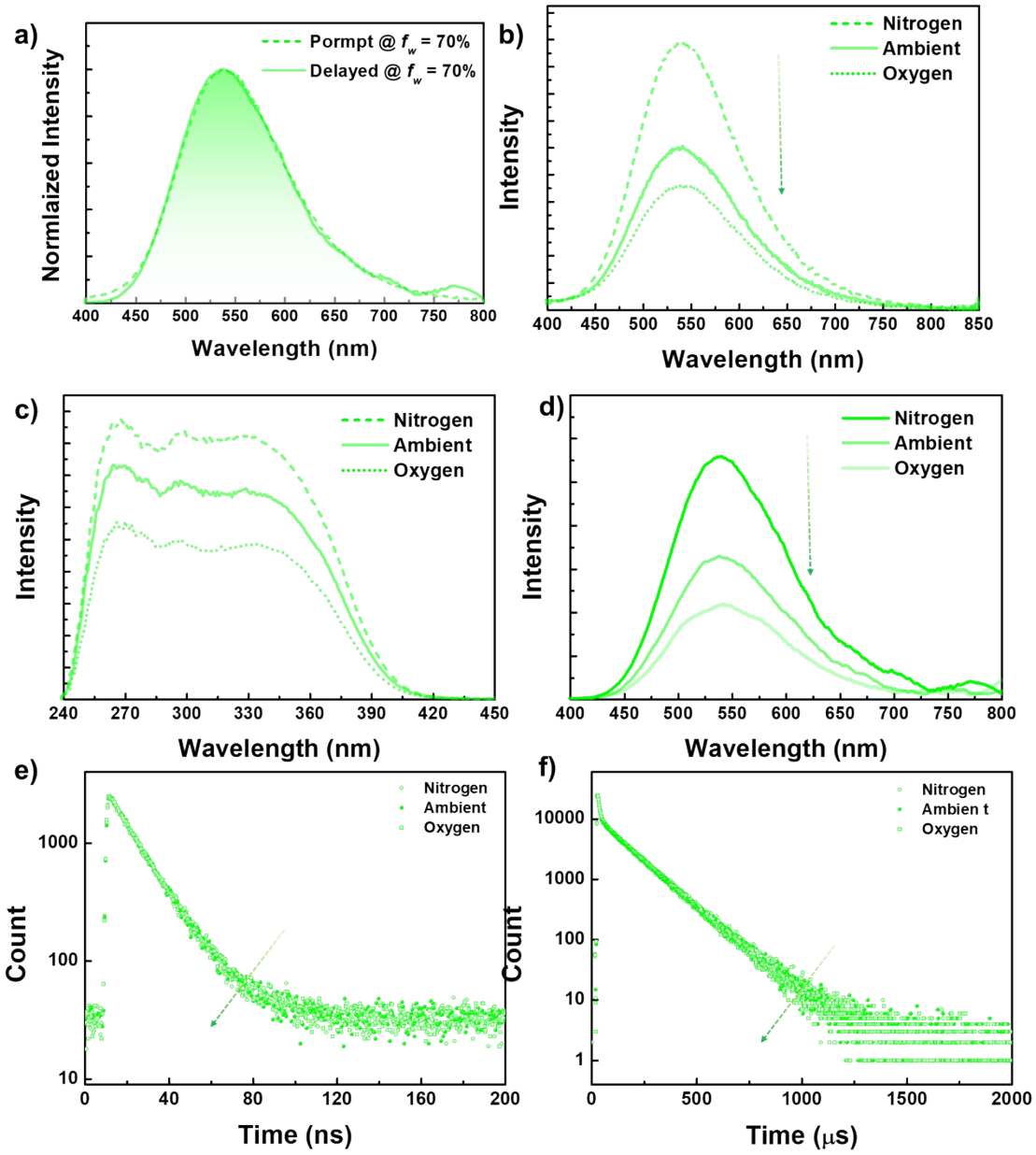

Figure S23. (a) Prompt and time-gated [20 μs delay] PL spectra for **BNO** in degassed DMSO-water mixture, f_w = 70%, (λ_{ex} = 310 nm). (b) Steady-state PL spectra, (c) excitation spectra, and (d) time-gated [20μs delay] PL spectra for BNO in DMSO-water mixture, fw = 70% under different environments (λ_{ex} = 310 nm). (e) Fluorescence and (d) delayed fluorescence decay plot for **BNO** in DMSO-water mixture, f_w = 70% (λ_{ex} = 310 nm; λ_{em} = 535 nm).

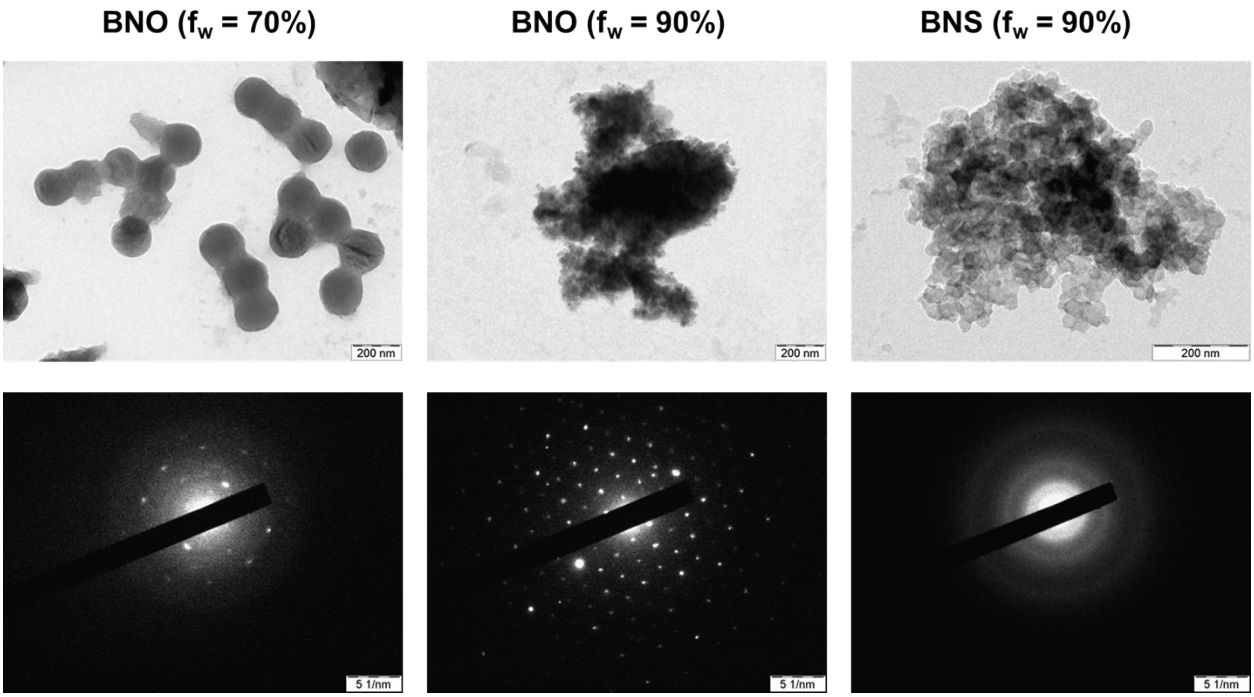

Figure S24. TEM images and corresponding selected area electron diffraction (SAED) pattern for aggregates of **BNO,** formed from DMSO-water mixture, f_w = 70%, 90%, and **BNS** at f_w = 90%

Table S8. Fl, DF lifetime, and total photoluminescence quantum yield for **BNO** in DMSO-water mixture, f_w = 70% and f_w = 90% (conc. 5x10^{-5} M) under different environments.

	λ_{ex} (nm)	λ_{em} (nm)	Fl		DF		PLQY
			$\tau_1(A_1)$	$\tau_2(A_2)$	$\tau_1(A_1)$	$\tau_2(A_2)$	
***f_w* = 70%**							
Nitrogen	310	535	14.58 ns (100 %)	-	60.07 µs (6.71 %)	146.04 µs (93.29 %)	0.25
Ambient	310	535	14.54 ns (100 %)	-	26.26 µs (3.28 %)	145.46 µs (96.72 %)	0.23
Oxygen	310	535	14.41 ns (100 %)	-	68.23 µs (7.74 %)	145.45 µs (92.26 %)	0.18
***f_w* = 90%**							
Nitrogen	310	580	10.39 ns (14.93 %)	15.64 ns (85.07 %)	24.98 µs (78.17 %)	109.49 µs (21.83 %)	0.19
Ambient	310	580			24.60 µs (83.24 %)	81.60 µs (16.76 %)	0.18
Oxygen	310	580	9.26 ns (57.53 %)	19.71 ns (42.47 %)	18.26 µs (68.99 %)	119.20 µs (31.01 %)	0.17

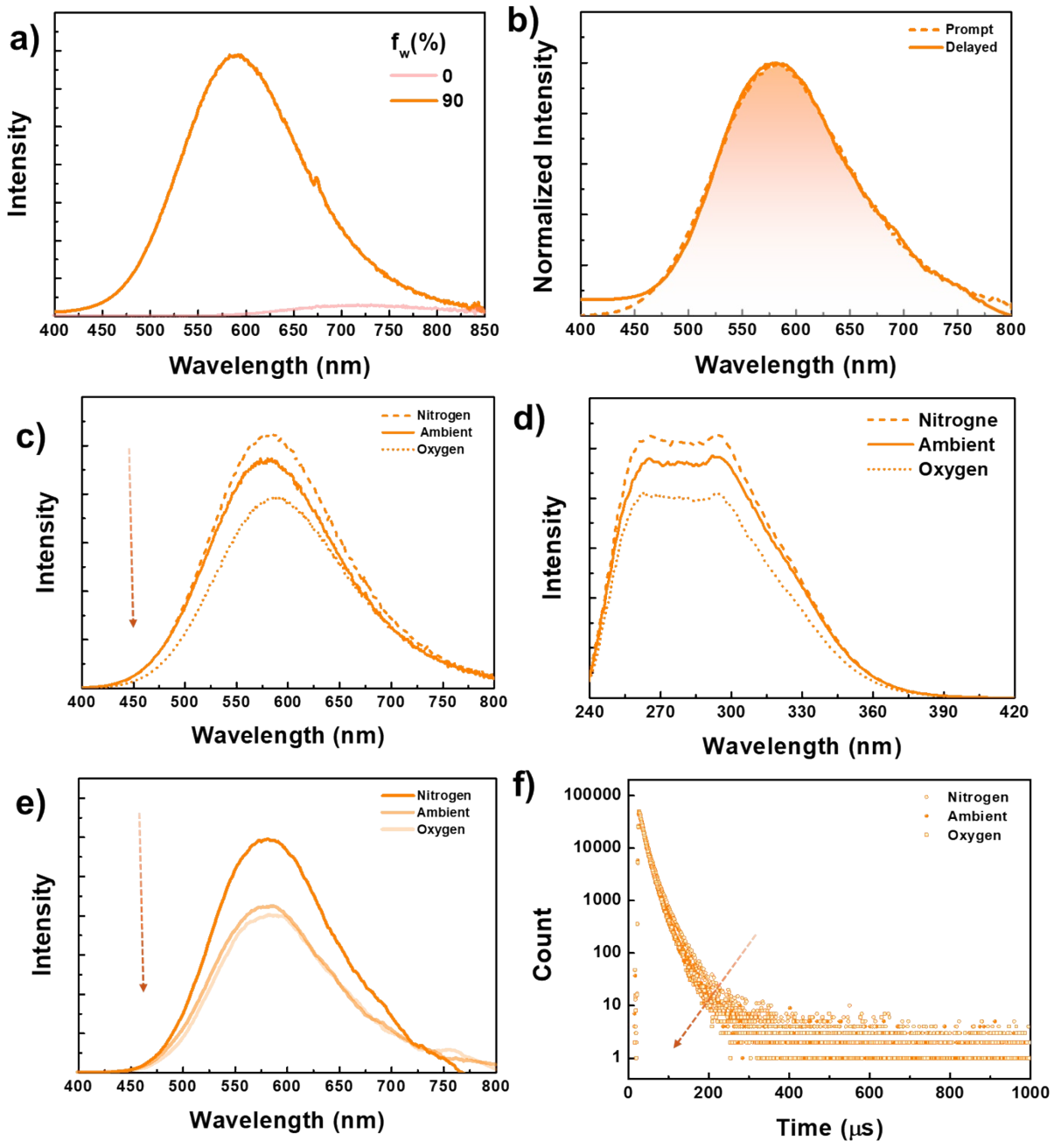

Figure S25. (a) Steady-state PL spectra of **BNS** in DMSO and DMSO-water mixture, f_w=*90%* (λ_{ex} = 280 nm). (b) Prompt and time-gated [20 μs delay] PL spectra for **BNS** in DMSO-water mixture, f_w = 90%, purged with nitrogen gas (λ_{ex} = 280 nm). (c) Steady-state PL spectra, (d) excitation spectra, and (e) Time-gated [20 μs delay] PL spectra for **BNS** in DMSO-water mixture, f_w = 90%, under different environments (λ_{ex} = 280 nm).(e) Fl, DF, decay plot for aggregates of **BNS** in DMSO-water mixture, f_w = 70% (conc. 5x10^{-5} M, λ_{ex} = 280 nm, and λ_{em} = 580 nm).

Table S9. Fl, DF lifetime, and total photoluminescence quantum yield for **BNS** in DMSO-water mixture, f_w = 90% under different environments (conc. 5x10^{-5} M) .

	λ_{ex} (nm)	λ_{em} (nm)	Fl		DF		PLQY
			$\tau_1(A_1)$	$\tau_2(A_2)$	$\tau_1(A_1)$	$\tau_2(A_2)$	
Nitrogen	280	580	10.31 ns (100 %)	-	13.52 µs (66.58 %)	32.96 µs (33.42 %)	0.32
Ambient	280	580	9.62 ns (100 %)	-	10.57 µs (63.21 %)	25.99 µs (36.79 %)	0.31
Oxygen	280	580	9.34 ns (100 %)	-	10.97 µs (66.29 %)	25.53 µs (33.71 %)	0.25

Table S10. Lifetime, PLQY values and corresponding radiative and nonradiative decay rate for **BNO** and **BNS** in degassed hexane and DMSO-water mixture [f_w = 70% and f_w = 90%] (conc. 5x10^{-5} M).

.

λ_{ex} [nm]	**λ_{em} [nm]**	**τ_{PF} [ns]**	**τ_{DF} [µs]**	**Φ_{Total}**	**Φ_{PF}**	**Φ_{DF} [%]**	**k_{PF} [$10^7 s^{-1}$]**	**k_{DF} [$10^3 s^{-1}$]**	**k_{ICS} [$10^7 s^{-1}$]**	**k_{rICS} [$10^4 s^{-1}$]**	**$k_{nr(S)}$ [$10^7 s^{-1}$]**
BNO (Hexane)											
310	605	13.60	6.38	12.0	1.2	10.80	0.88	16.9	6.6	15.67	6.47
BNO (DMSO-Water: f_w =70%)											
310	535	14.41	140.27	25.0	18.1	6.9	12.41	0.49	1.89	0.10	37.24
BNO (DMSO-Water: f_w =90%)											
310	580	14.08	43.42	19.2	17.1	2.1	12.14	0.48	0.77	0.25	51.11
BNS (DMSO-Water: f_w =90%)											
280	580	10.31	20.02	0.32	0.25	0.7	2.46	3.09	1.90	6.21	5.3.3

τ_{PF} and τ_{DF} are the average fluorescence and delayed fluorescence lifetime. Φ_{Total} is total PLQY, $\Phi_{PF,}$ and Φ_{DF} PLQY for prompt and delayed fluorescence, k_{PF}, k_{DF}, k_{ICS}, k_{rISC} $k_{nr(s)}$ are the rate fluorescence decay, delayed fluorescence decay, intersystem crossing, reverse intersystem crossing, non-radiative decay from singlet respectively. λ_{ex} and λ_{em} are the excitation and emission wavelengths, respectively.

The equation for Calculating Delayed Fluorescence Rate Constance in solution [5]

$$k_r^{PF} = \frac{\phi_{PF}}{\tau_{PF}}$$

$$k_r^{DF} = \frac{\phi_{DF}}{\tau_{DF}}$$

$$k_{Total}^{PF} = \frac{1}{\tau_{PF}}$$

$$k_{Total}^{DF} = \frac{1}{\tau_{DF}}$$

$$k_{nr}^{ISC} = \frac{\phi_{DF}\, k_{Total}^{PF}}{\phi_{total}}$$

$$k_{nr}^{rISC} = \frac{\phi_{DF}\, k_{Total}^{PF}\, k_{Total}^{DF}}{k_{nr}^{ISC}\, \phi_{PF}}$$

$$k_{nr}^{S} = \frac{1}{\tau_{PF}} - (k_r^{PF} + k_{nr}^{ISC})$$

$k_{Total}^{PF} = Total\ deacy\ Rate\ of\ \ prompt\ component$

$k_{Total}^{DF} = Total\ decay\ rate\ of\ delayed\ component$

$k_r^{PF} = Radiative\ decay\ rate\ of\ prompt\ component$

$k_r^{DF} = Radiative\ decay\ rate\ of\ delayed\ component$

$k_{nr}^{ISC} = Rate\ of\ intersystem\ crossing$

$k_{nr}^{rISC} = Rate\ of\ reverse\ intersystem\ crossing$

$k_{nr}^{S} = Non\ radiative\ decay\ rate\ from\ S_1$

$\tau_{PF} = Lifetime\ of\ Prompt\ component$

$\tau_{DF} = Lifetime\ of\ Prompt\ component$

$\phi_{total} = Total\ photoluminscence\ quantum\ yield$

$\phi_{PF} = Prompt\ fluorescence\ quantum\ yield$

$\phi_{DF} = Deleyed\ fluorescence\ quantum\ yield$

5.2 Solid-state photoluminescence studies

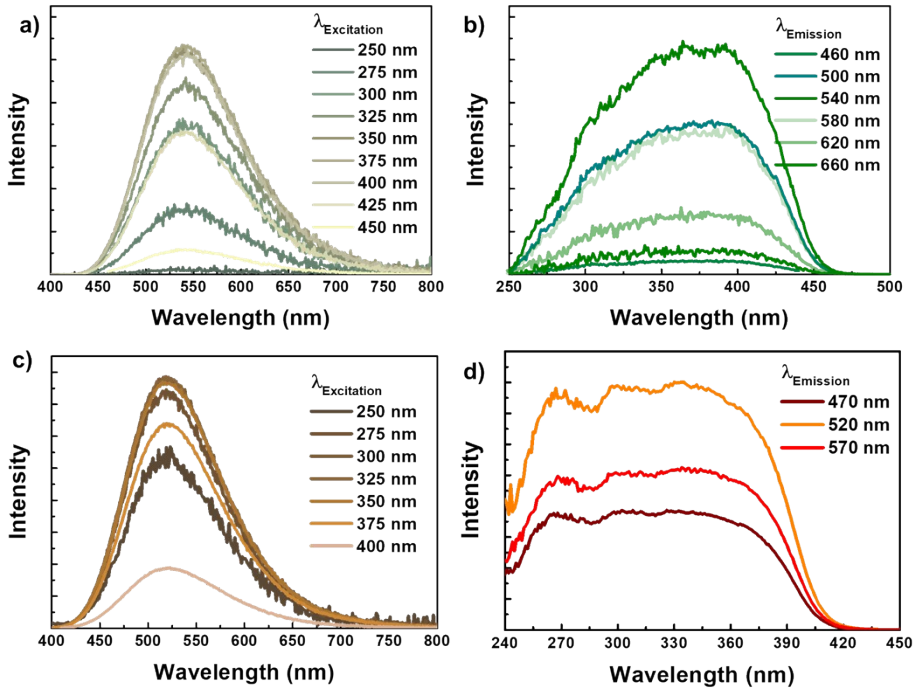

Figure S26. Figure S26. Excitation-dependent PL and corresponding excitation spectra of (a and b) **BNO** and (c and d) **BNS**.

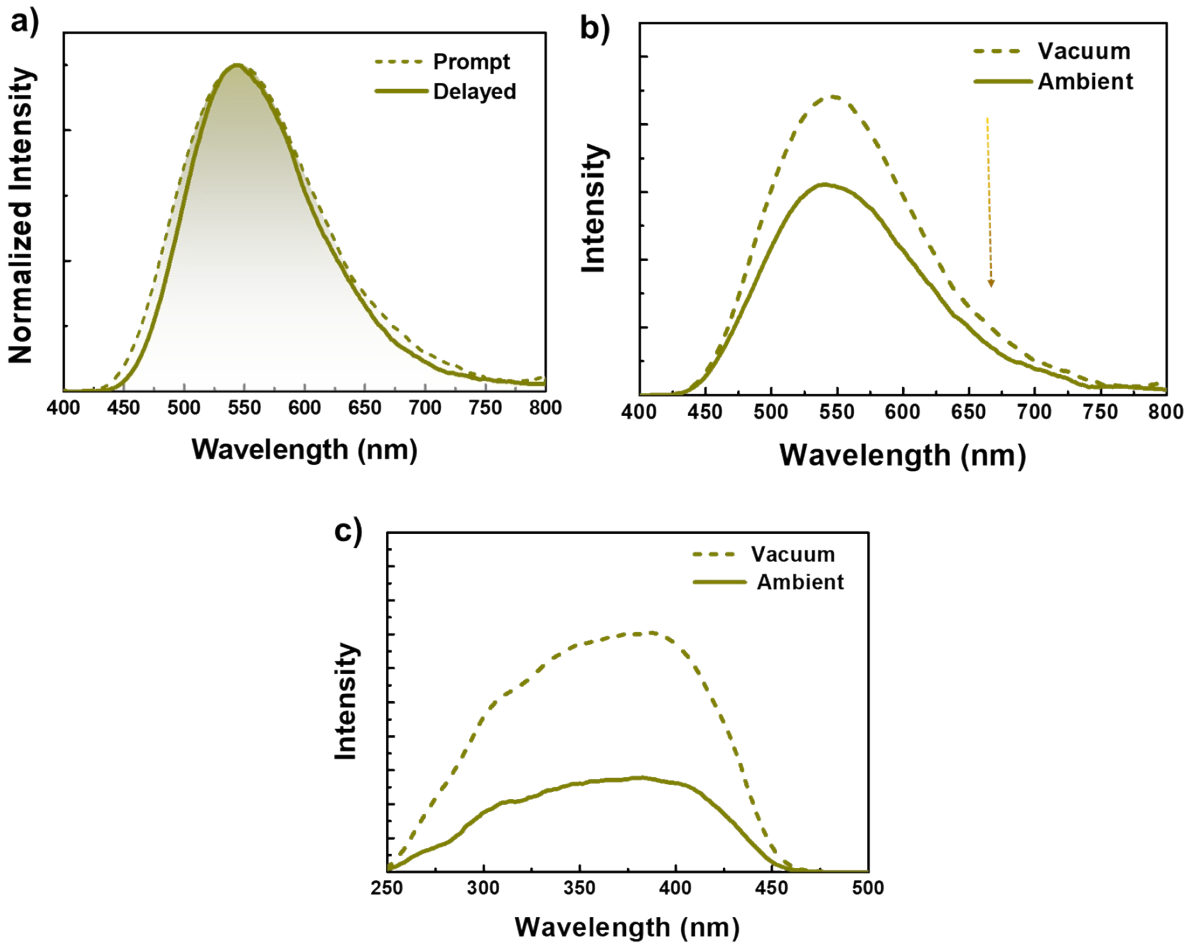

Figure S27. (a) Prompt and time-gated [50 μs delay] PL spectra for the solids of **BNO** at 298 K under ambient conditions (λ_{ex} = 375 nm). (b) Steady-state PL spectra, (c) excitation spectra, for the solids of **BNO** at 298 K under vacuum (absence of O_2) and ambient (presence of O_2) (λ_{ex} = 375 nm).

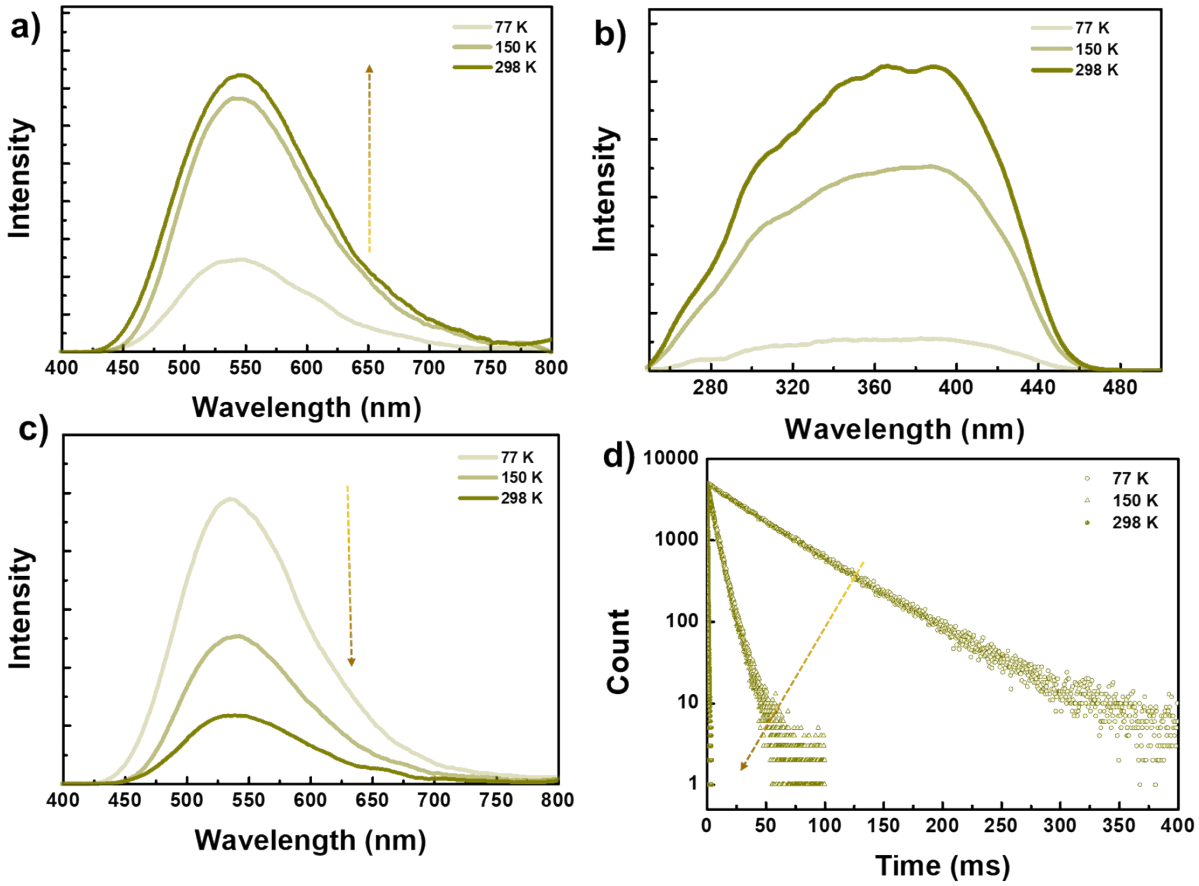

Figure S28. (a) Steady-state PL, (b) excitation spectra, (c) time-gated PL spectra, and (d) DF decay [λ_{em} = 540 nm] plot for the solids of **BNO** at a different temperature under vacuum (absence of O_2) (λ_{ex} = 375 nm).

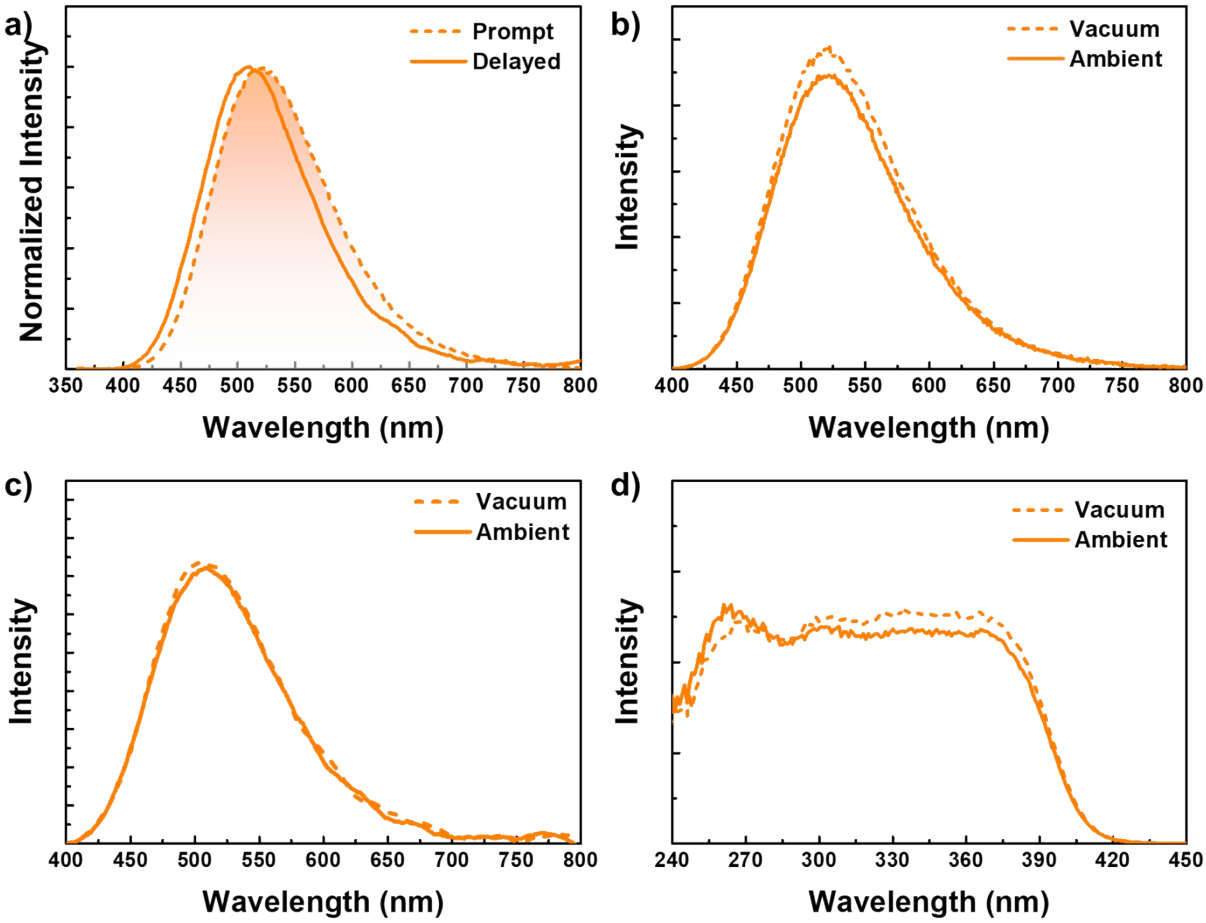

Figure S29. (a) Prompt and time-gated/delayed [50 μs delay] PL spectra for the solids of **BNS** at 298 K under ambient conditions (λ_{ex} = 350 nm). (b) Steady-state PL spectra, (c) time-gated [50μs delay] PL, and (d) excitation spectra [λ_{em} = 520 nm] for the solids of **BNS** at 298 K under vacuum (absence of O_2) and ambient (presence of O_2) (λ_{ex} = 375 nm).

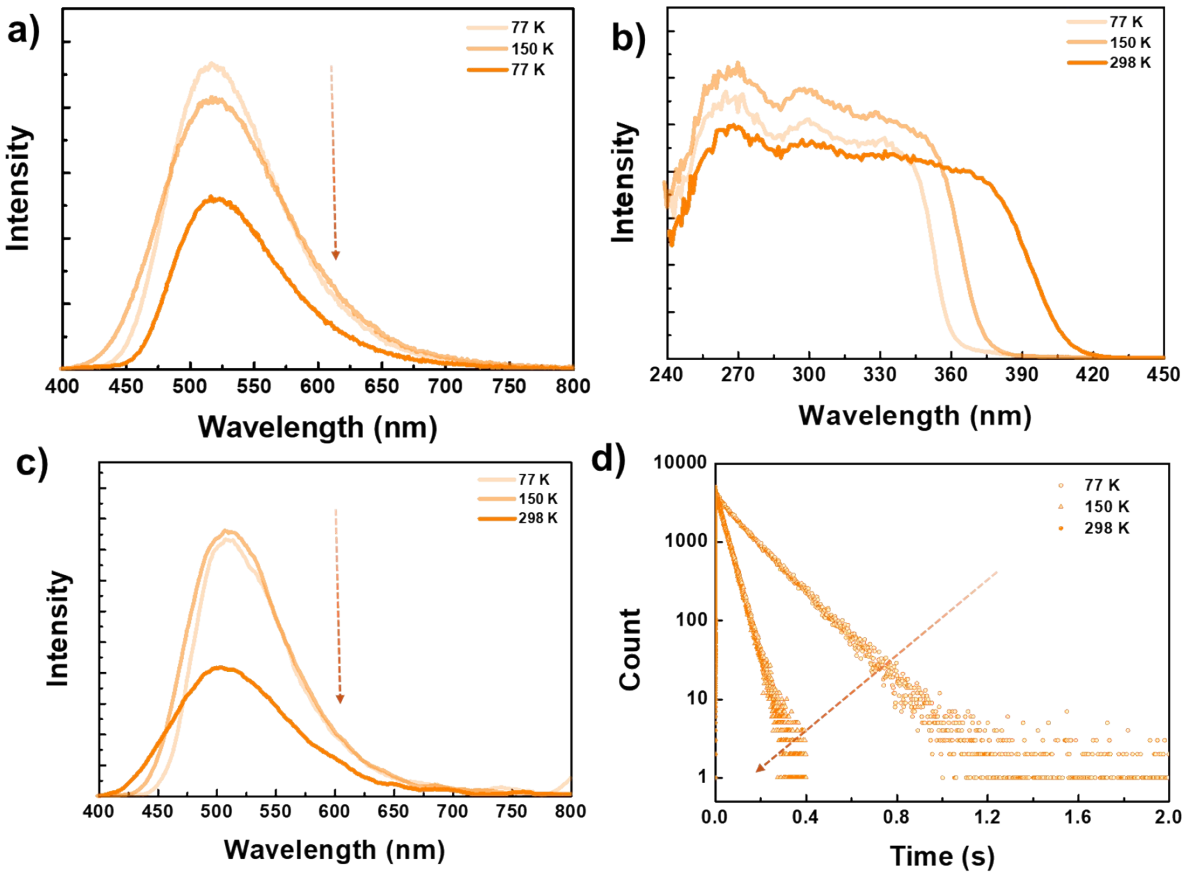

Figure S30. (a) Steady-state PL spectra (b) excitation spectra, (c) time-gated PL spectra, and (e) phosphorescence decay plot [λ_{em} = 500 nm] for the solids of **BNS** at a different temperature under vacuum (absence of O_2) (λ_{ex} = 350 nm).

Table S11. Fl and DF/Phosphorescence (PH)* lifetime for the solids of **BNO** and **BNS** at different temperatures under vacuum (absence of O_2) and ambient conditions (298 K).

Temperature (K)	λ_{ex} (nm)	λ_{em} (nm)	Fl lifetime		DF /PH* lifetime		
			$\tau_1(A_1)$	$\tau_2(A_2)$		$\tau_1(A_1)$	$\tau_2(A_2)$
BNO							
77	375	540	13.90 ns (100 %)	-	540	38.12 ms (39.14 %)	55.76 ms (60.86 %)
150	375	540	13.71 ns (100 %)	-	540	5.18 ms (61.43 %)	9.13 ms (38.57 %)
298 (Vacuum)	375	540	14.43 ns (100 %)	-	540	219.81 µs (11.20%)	327.82 µs (88.80%)
298 (Ambient)	375	540	13.92 ns (100%)		540	131.06 µs (46.17 %)	181.07 µs (23.83 %)
BNS							
77	375	520	2.35 ns (37.15 %)	9.74 ns (62.85 %)	505*	31.62 ms (1.81 %)	146.18 ms(98.19 %)
150	375	520	8.99 ns (100 %)	-	505*	41.16 ms (100 %)	-
298 (Vacuum)	375	520	9.94 ns (100 %)	-	500*	91.38 µs (100 %)	-
298 (Ambient)	375	520	9.87 ns (100%)		500*	91.03 µs (100 %)	-

5.4 Photoluminescence of films (doped in polymer and neat) of BNO and BNS

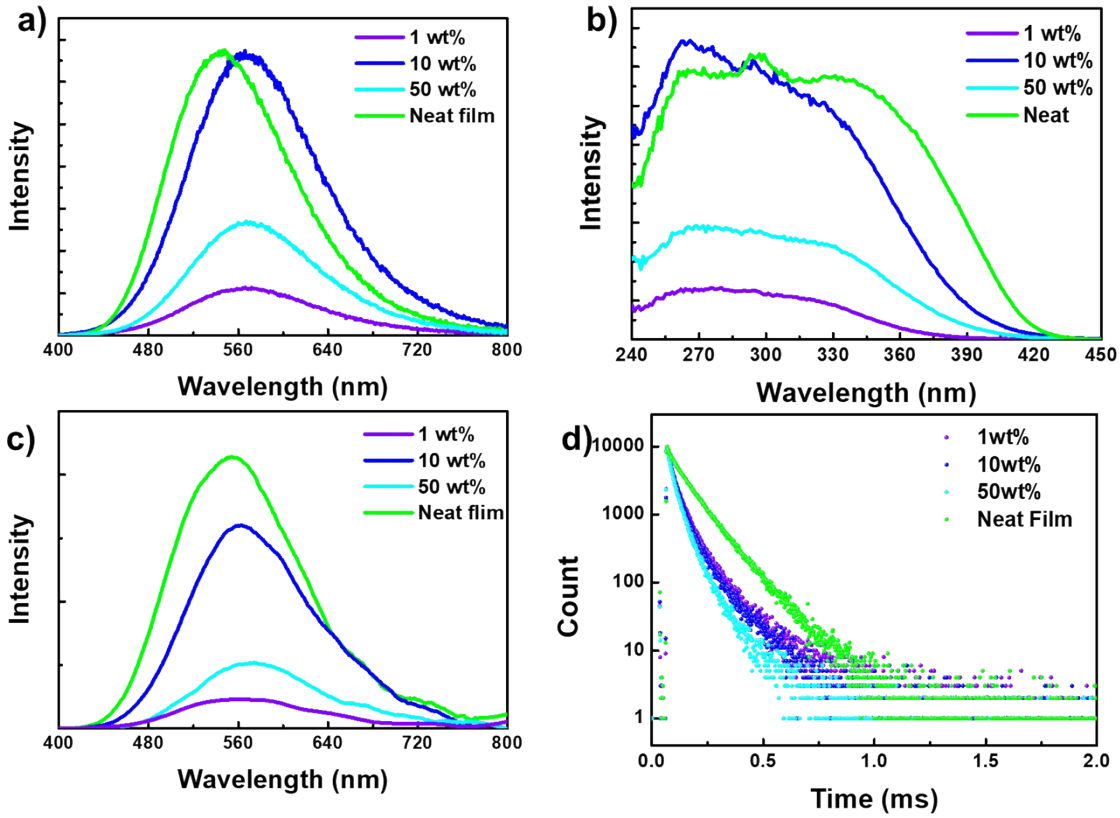

Figure S31. (a, b) Steady-state PL and corresponding excitation spectra for **BNO** doped in PMMA with different loading concentrations and corresponding neat film (λ_{ex} = 330 nm respectively. (c) Time gated /Delayed spectra [50 μs delay] PL spectra and (d) delayed fluorescence decay under vacuum atmosphere at 298 K for **BNO** doped in PMMA with different loading concentration and corresponding neat film (λ_{ex} = 330 nm, λ_{em} = 568 nm for doped film and 545 nm for neat film).

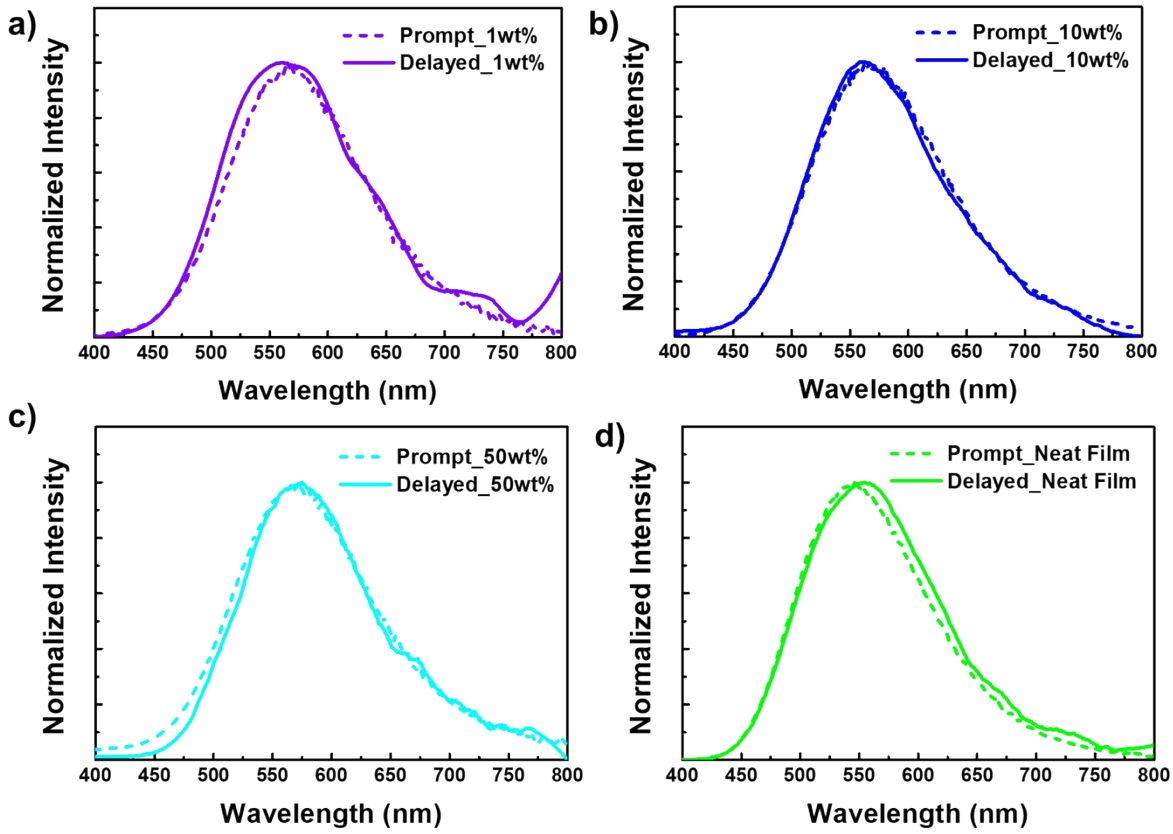

Figure S32. Prompt and time-gated/delayed [50 μs delay] PL spectra for **BNO** doped in PMMA with doping concentration (a) 1wt%, (b) 10wt%, (c) 50wt% and as neat film at λ_{ex} = 330 nm

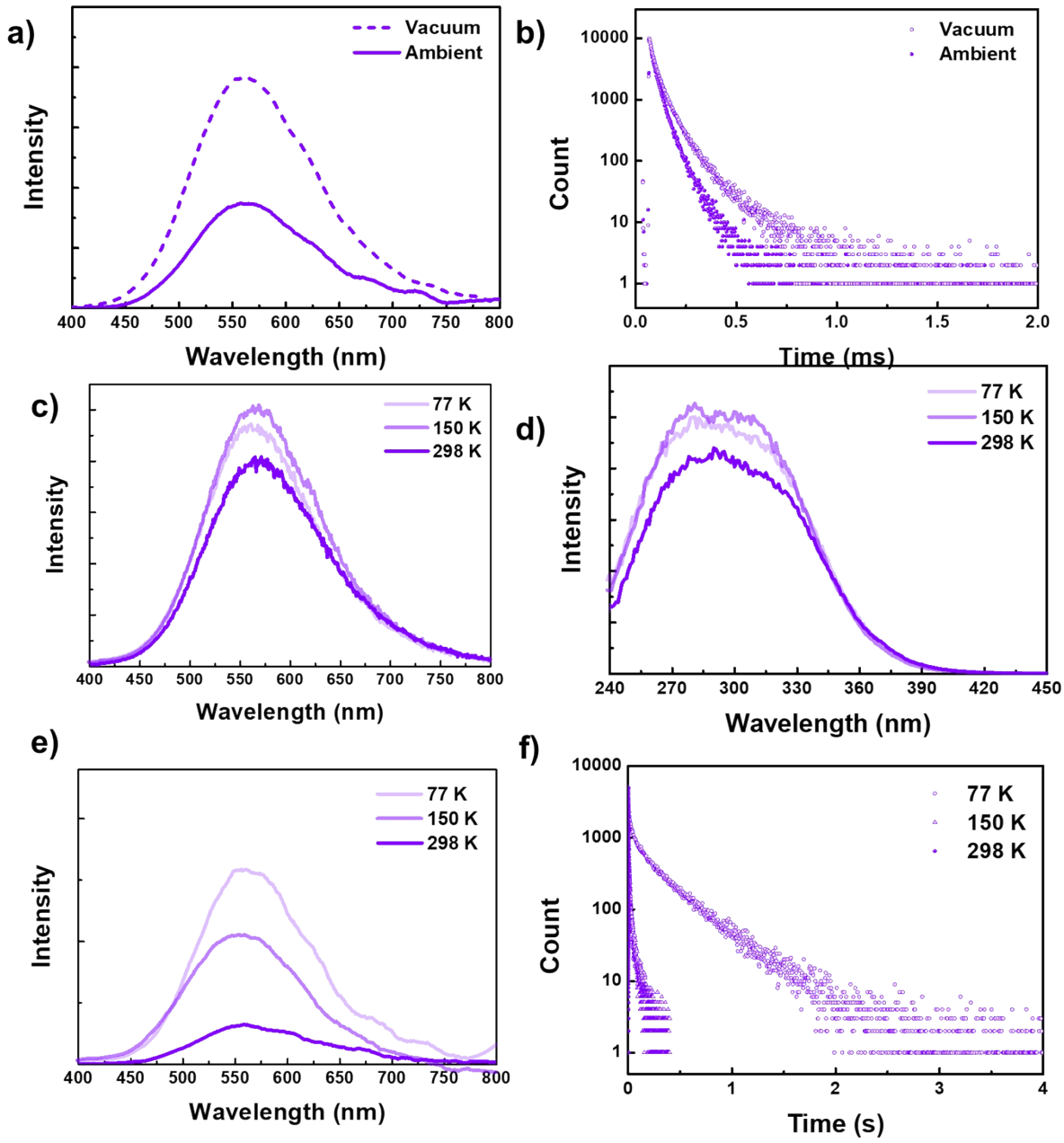

Figure S33. (a) Time-gated/delayed [50μs delay] PL spectra and (b) delayed fluorescence decay [λ_{em} = 540 nm] for **BNO** doped in PMMA (1wt%) at 298 K under vacuum (absence of O_2) and ambient (presence of O_2) at λ_{ex} = 330 nm, (c) Steady-state PL spectra, (d) excitation spectra, (e) time-gated/delayed [50μs delay] PL spectra, and (f) delayed fluorescence decay for **BNO** doped in PMMA (1wt%) at λ_{ex} = 330 nm and λ_{em} = 540 nm under vacuum at different temperatures.

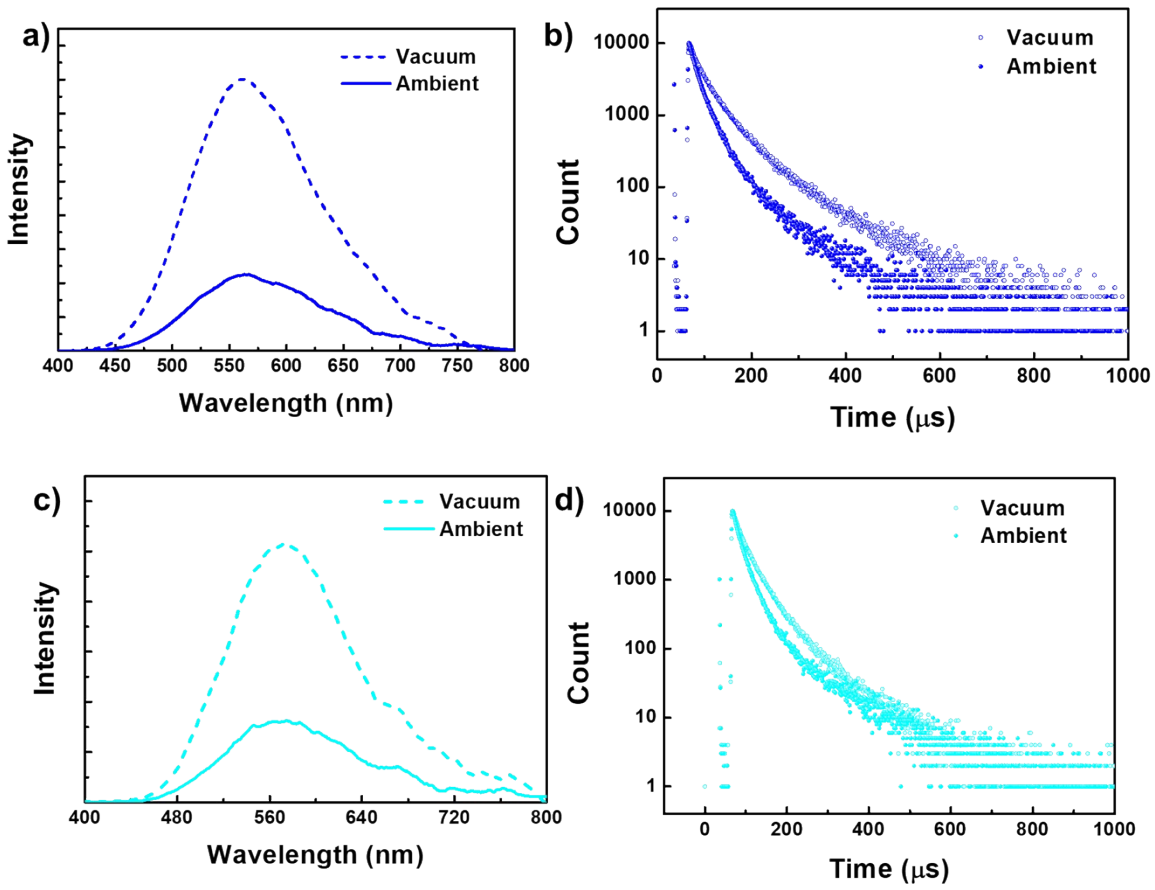

Figure S34. (a, c) Time-gated/delayed [50μs delay] PL spectra and (b, d) delayed fluorescence decay [λ_{em} = 540 nm] for **BNO** doped in PMMA with doping concentrations (a,b)10 wt% (c,d) 50 wt% at 298 K under vacuum (absence of O_2) and ambient (presence of O_2) at λ_{ex} = 330 nm.

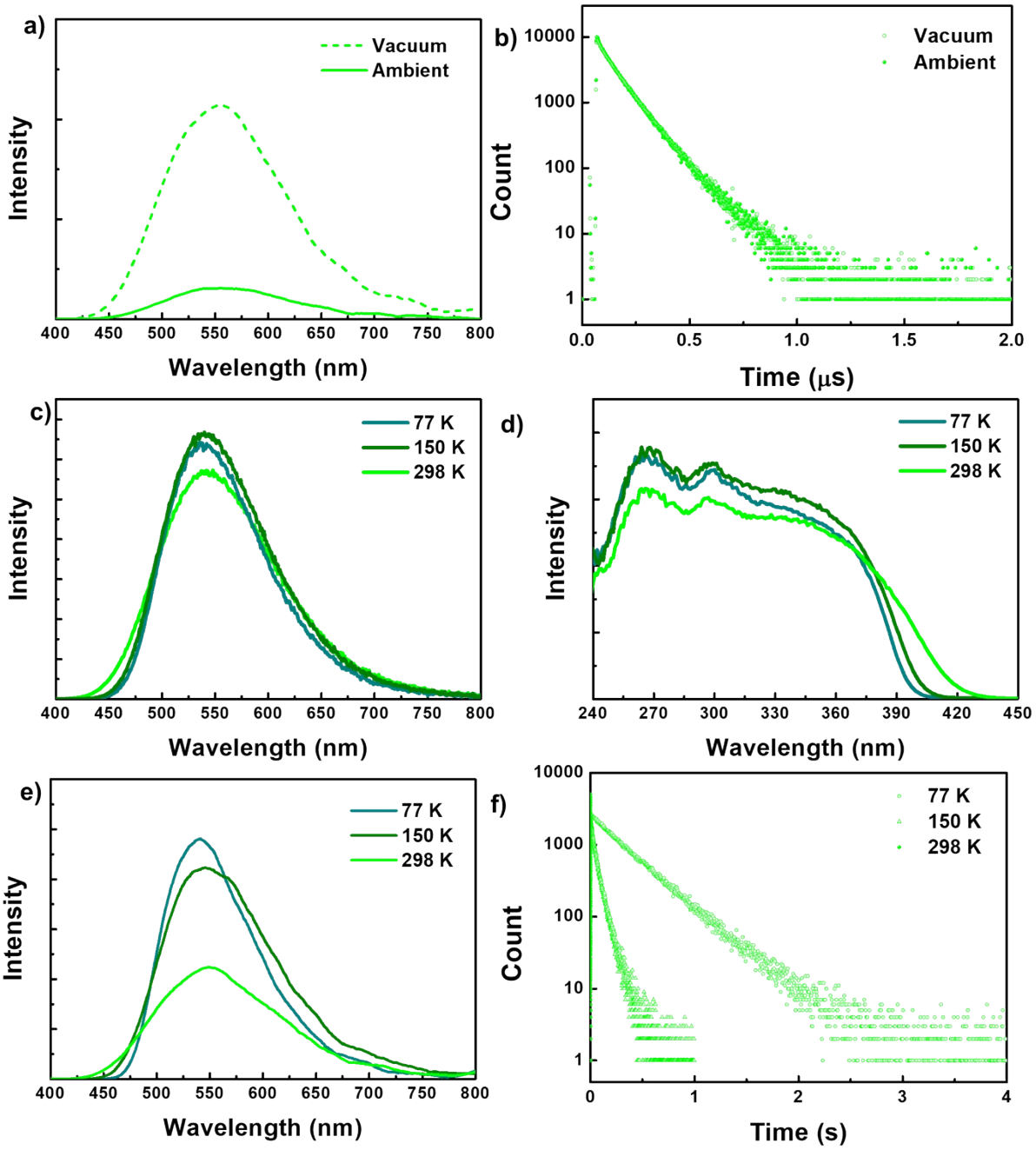

Figure S35.(a) Time-gated/delayed [50μs delay] PL spectra and (b) delayed fluorescence decay [λ_{em} = 545 nm] for the neat film of **BNO** at 298 K under vacuum (absence of O_2) and ambient (presence of O_2) at λ_{ex} = 330 nm. (c) Steady-state PL spectra, (e) excitation spectra, (e) time-gated/delayed [50μs delay] PL spectra, and (e) delayed fluorescence decay for the neat film of **BNO** at λ_{ex} = 330 nm and λ_{em} = 545 nm under vacuum at different temperature.

Table S12. Fluorescence (Fl) and Delayed fluorescence (DF) lifetime for **BNO** doped in PPMA with different loading concentrations and corresponding neat film at 298 K under vacuum (absence of O_2) and ambient (presence of O_2).

		Fluorescence lifetime					Delayed fluorescence lifetime		PLQY
		λ_{ex} (nm)	λ_{em} (nm)	$\tau_1(A_1)$	$\tau_2(A_2)$	λ_{em} (nm)	$\tau_1(A_1)$	$\tau_2(A_2)$	
1wt%	Vac	310	568	16.32 ns (100 %)	-	568	38.97 µs (62.45 %)	122.04 µs (37.55 %)	0.30
	Ambi	310	568	15.92 ns (100%)		568	25.81 µs (62.65 %)	68.17 µs (37.35 %)	
10wt%	Vac	310	568	17.06 ns (100%)		568	29.99 µs (59.39 %)	93.48 µs (40.61 %)	0.48
	Ambi	310	568	16.85 ns (100%)		568	20.84 µs (75.09 %)	76.91 µs (24.91 %)	
50wt%	Vac	310	568	16.67 ns (100%)		568	27.04 µs (64.26 %)	77.94 µs (35.74 %)	0.50
	Ambi	310	568	16.53 ns (100%)		568	21.35 µs (77.83 %)	93.15 µs (22.17 %)	
Neat	Vac	310	545	14.40 ns (100%)		545	73.74 µs (52.25 %)	130.38 µs (47.75 %)	0.63
	Ambi	310	545	14.02 ns (100%)		545	65.05 µs (41.70 %)	123.32 µs (58.30 %)	

Table S13. Fluorescence (Fl) and Delayed fluorescence (DF) lifetime for **BNO** doped in PPMA (1wt%) and corresponding neat film at different temperatures under vacuum (absence of O_2).

.

Temperature	Fluorescence lifetime				Delayed fluorescence lifetime		
	λ_{ex} (nm)	λ_{em} (nm)	$\tau_1(A_1)$	$\tau_2(A_2)$	λ_{em} (nm)	$\tau_1(A_1)$	$\tau_2(A_2)$
1wt%							
77 K	310	568	20.02 ns (100)	-	568	67.01 ms (18.89 %)	146.18 ms (81.11 %)
150 K	310	568	19.07 ns (100 %)	-	568	5.69 ms (50.45 %)	39.18 ms (49.55 %)
298 K	310	568	16.32 ns (100 %)	-	568	38.97 µs (62.45 %)	122.04 µs (37.55 %)
Neat Film							
77 K	310	545	12.33 ns (100)	-	560	100.1 ms (3.95 %)	349.97 ms (96.05 %)
150 K	310	545	13.16 ns (100 %)	-	560	23.62 ms (35.57 %)	69.31 ms (64.43 %)
298 K	310	545	14.40 ns (100%)		545	73.74 µs (52.25 %)	130.38 µs (47.75 %)

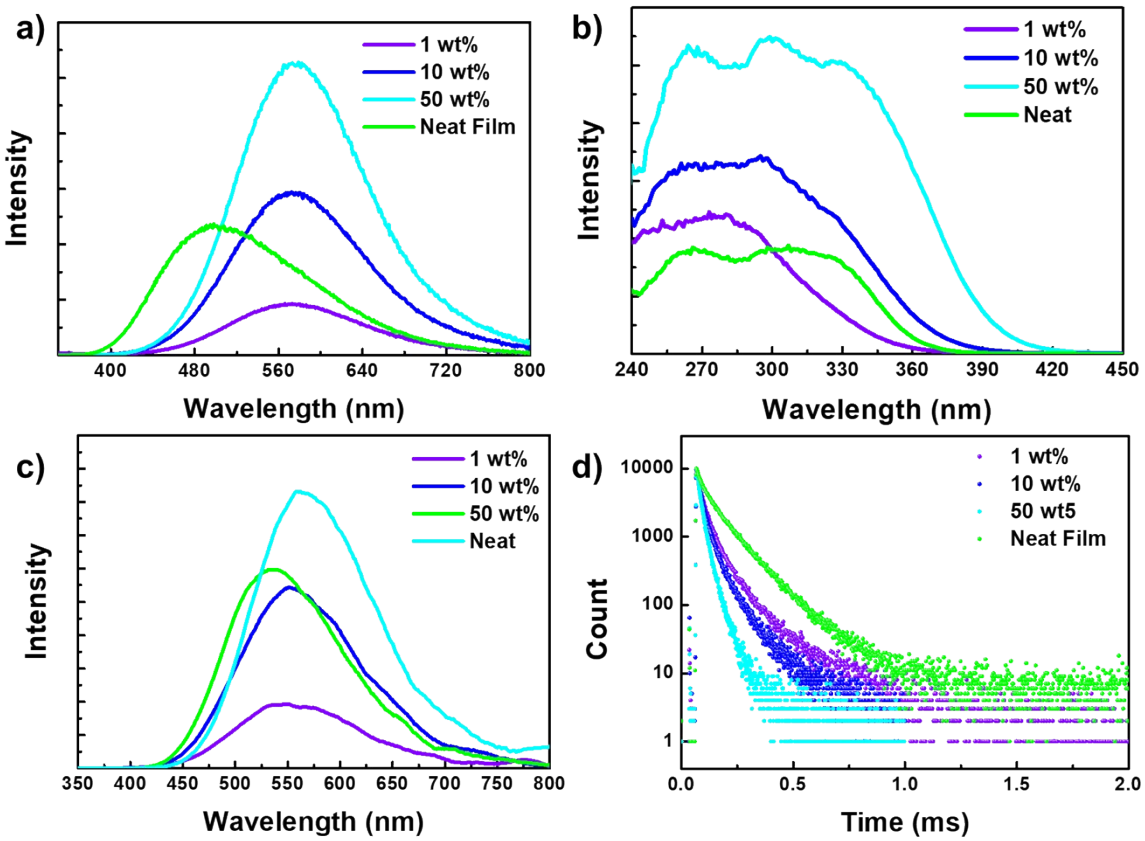

Figure S36. (a, b) steady-state PL and corresponding excitation spectra for **BNS** doped film in PPMA with different loading concentrations and corresponding neat film (λ_{ex} = 330 nm respectively. (c) Time gated /Delayed spectra [50 μs delay] PL spectra and (d) phosphorescence decay under vacuum atmosphere at 298 K for **BNS** doped film in PPMA with different loading concentrations and corresponding neat film (λ_{ex} = 330 nm, λ_{em} = 550, 555, 565 for doped film 1wt%, 10wt% and 50wt% respectively and 535 for neat film).

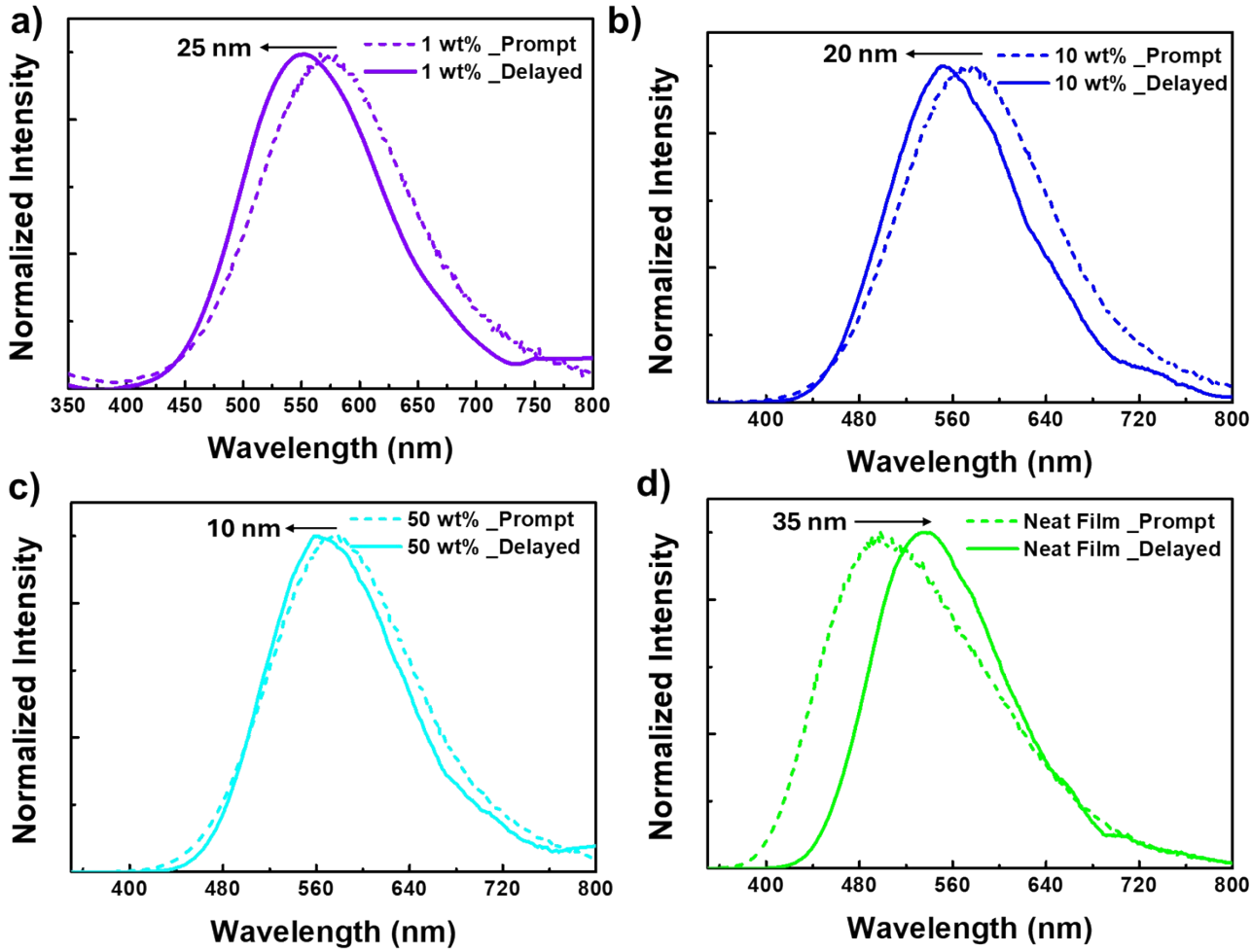

Figure S37. Prompt and time-gated/delayed [50 μs delay] PL spectra for **BNS** doped film in PMMA with doping concentration (a) 1wt%, (b) 10wt%, (c) 50wt% and as neat film at λ_{ex} = 330 nm

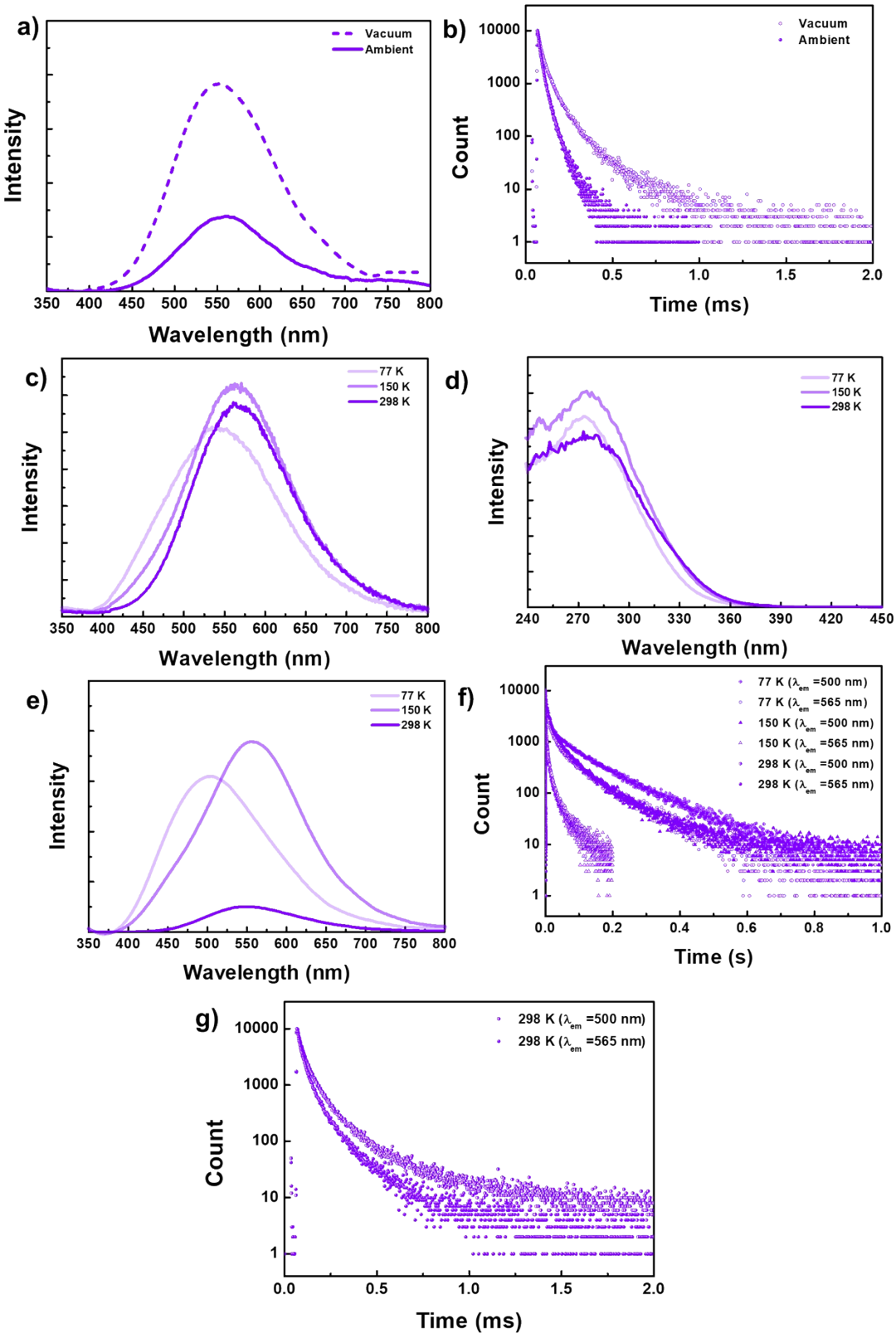

Figure S38. (a) Time-gated/delayed [50µs delay] PL spectra and (b) delayed fluorescence decay [λ_{em} = 540 nm] for **BNS** doped in PMMA (1wt%) at 298 K under vacuum (absence of O_2) and ambient (presence of O_2) at λ_{ex} = 330 nm (c) Steady-state PL spectra, (d) excitation spectra, (e) time-gated/delayed [50µs delay] PL spectra and (f) delayed fluorescence decay for **BNS** doped in PMMA (1wt%) at λ_{ex} = 330 nm and λ_{em} = 540 nm under vacuum at different temperature

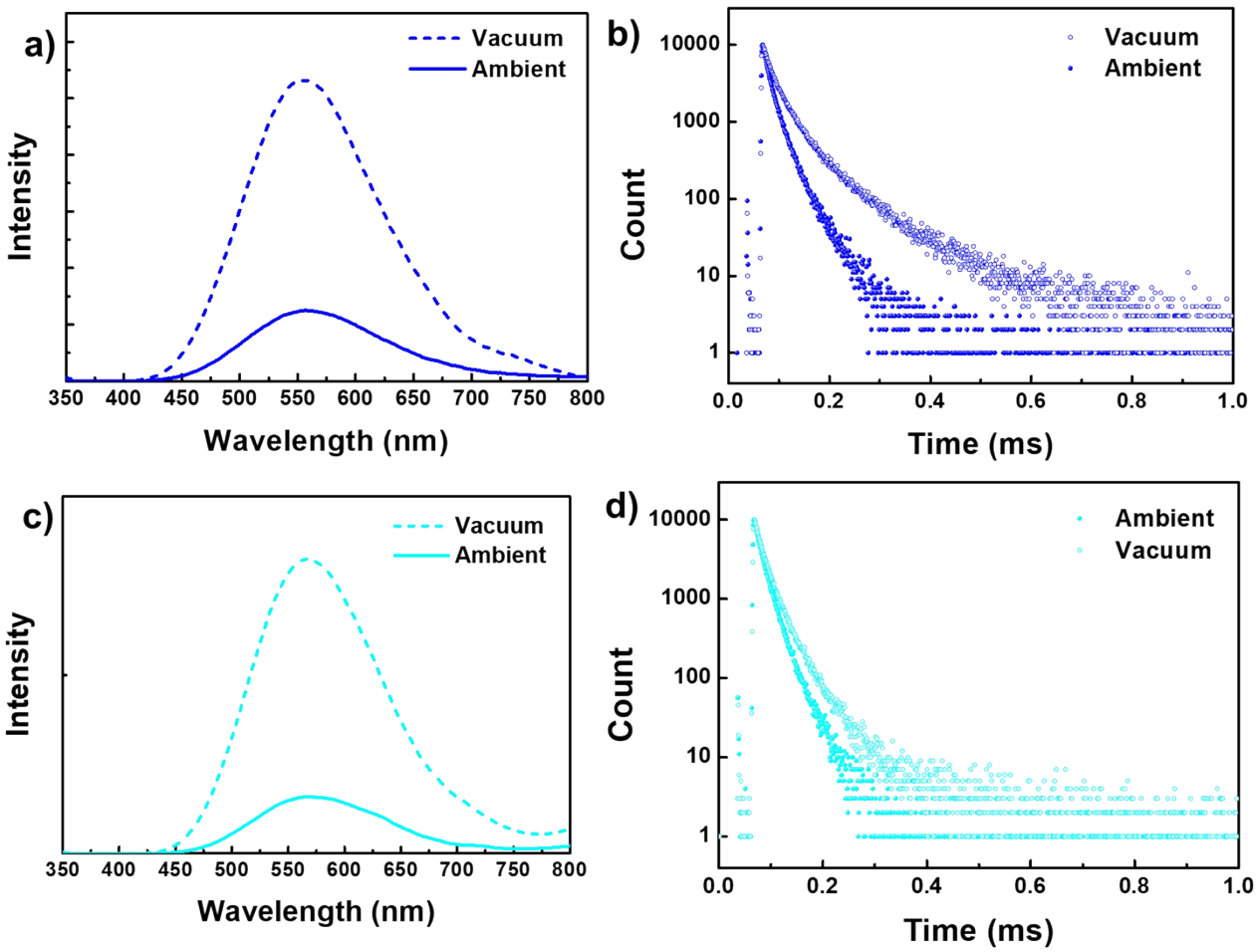

Figure S39. (a, c) Time-gated/delayed [50µs delay] PL spectra and (b, d) phosphorescence decay [λ_{em} = 540 nm] for **BNS** doped in PMMA with doping concentrations (a,b)10 wt% (c,d) 50 wt% at 298 K under vacuum (absence of O_2) and ambient (presence of O_2) at λ_{ex} = 330 nm.

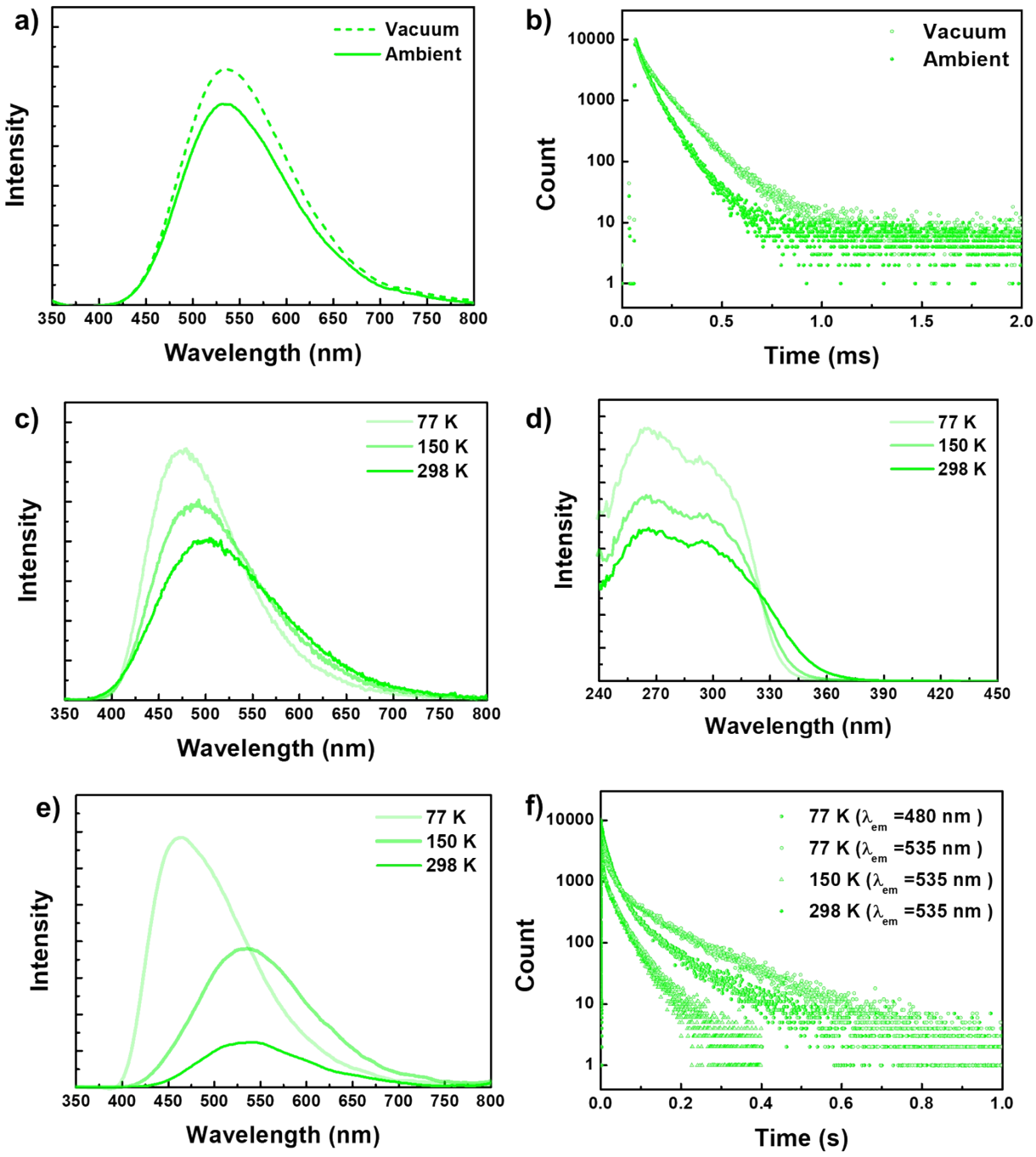

Figure S40. (a) Time-gated/delayed [50µs delay] PL spectra and (b) delayed fluorescence decay [λ_{em} = 540 nm] for neat film of **BNS** at 298 K under vacuum (absence of O_2) and ambient (presence of O_2) at λ_{ex} = 330 nm, (c) Steady-state PL spectra, (e) excitation spectra, (e) time-gated/delayed [50µs delay] PL spectra, and (e) phosphorescence decay for neat film of **BNS** at λ_{ex} = 330 nm and λ_{em} = 540 nm under vacuum at different temperature.

Table S14 Fluorescence (Fl) and Delayed fluorescence (DF) lifetime for **BNS** doped in PPMA with different loading concentrations and corresponding neat film at 298 K under vacuum (absence of O_2) and ambient (presence of O_2).

		Fluorescence lifetime				Phosphorescence lifetime			PLQY
		λ_{ex} (nm)	λ_{em} (nm)	τ_1 (A_1)	τ_2 (A_2)	λ_{em} (nm)	τ_1 (A_1)	τ_2 (A_2)	
1wt%	Vac	310	575	12.79 ns (100%)		550	32.65 µs (63.55 %)	132.54 µs (36.45 %)	0.41
	oxy	310	575	12.26 ns (100%)		550	18.05 µs (66.55 %)	52.90 µs (33.45 %)	
10wt%	Vac	310	575	12.63 ns (100%)		555	24.57 µs (61.58 %)	88.39 µs (38.42 %)	0.54
	oxy	310	575	12.62 ns (100%)		555	13.43 µs (59.29 %)	36.36 µs (40.71 %)	
50wt%	Vac	310	575	12.78 ns (100%)		565	16.01 µs (64.97 %)	43.37 µs (35.03 %)	0.87
	oxy	310	575	12.67 ns (100%)		565	15.65 µs (70.33 %)	36.30 µs (29.67 %)	
Neat	Vac	310	500	9.04 ns (100%)		535	52.33 µs (29.63 %)	133.04 µs (70.37 %)	0.60
	oxy	310	500	8.71 ns (100%)		535	44.97 µs (47.69 %)	99.13 µs (52.31 %)	

Table S15. Fluorescence (Fl) and Delayed fluorescence (DF) lifetime for **BNO** doped in PPMA (1wt%) and corresponding neat film at different temperatures under vacuum (absence of O_2).

Temperature	Fluorescence lifetime				Phosphorescence lifetime		
	λ_{ex} (nm)	λ_{em} (nm)	τ_1 (A_1)	τ_2 (A_2)	λ_{em} (nm)	τ_1 (A_1)	τ_2 (A_2)
1wt%							
77 K	310	540	15.28 ns (100) -	-	500 565 620	23.44 ms (20.17 %) 17.10 ms (32.99 %) 14.37 ms (36.75 %)	131.10 ms (79.83 %) 108.89 ms (67.01 %) 100.11 ms (63.25 %)
150 K	310	567	13.42 ns (100 %)	-	550 480	4.06 ms (45.18%) 19.67 ms (37.00 %)	27.32 ms (54.82%) 94.95 ms (63.0 %)
298 K	310	575	12.79 ns (100%)		550 500 600	32.65 µs (63.55 %) 48.83 µs (62.40 %) 35.73 µs (62.87 %)	132.54 µs (36.45 %) 194.53 µs (37.60 %) 131.16 µs (37.13 %)
Neat film							
77 K	310	475	9.22 ns (100)	-	462 520	18.24 ms (64.62 %) 20.23 ms (34.63)	93.55 ms (35.38 %) 124.92 ms (65.37)
150 K	310	488	9.08 ns (100 %)	-	460 540 585	7.25 ms (21.01 %) 11.94 ms (26.71%) 3.40 ms (32.56%)	38.57 ms (78.99) 41.63 ms (73.29) 29.99 ms (67.44)
298 K	310	500	9.04 ns (100%)		535 580	52.33 µs (29.63 %) 28.84 µs (36.21 %)	133.04 µs (70.37 %) 86.37 µs (63.79 %)

5.5 Excited State Theoretical Studies

Table S16. The bond parameters for **BNS** and **BNO** obtained from the ground state (S_0) and excited state (S_1, T_1, T_5, T_6) optimized geometry using a DFT or TD-DFT calculation with B3LYP/6-31G(d) level of theory.

State	B-N bond length (Å)	Dihedral angle (deg)	The angle between the xylyl plane(deg)	The angle between the phenyl plane in phenoxazine/phenothiazine (deg)	Dipol moment
BNO					
S0	1.444	23.92	84.59	146.59	0.82
S1	1.619	69.42	72.01	174.51	6.56
T1	1.605	60.06	73.35	178.34	7.0
T5	1.485	42.97	71.21	161.45	1.62
BNO					
S0	1.446	18.96	81.51	135.86	1.30
S1	1.630	68.94	70.15	172.92	3.43
T1	1.617	62.80	71.16	178.08	7.37
T5	1.498	43.70	78.27	151.66	1.78
T6	1.512	51.38	81.15	153.80	1.69

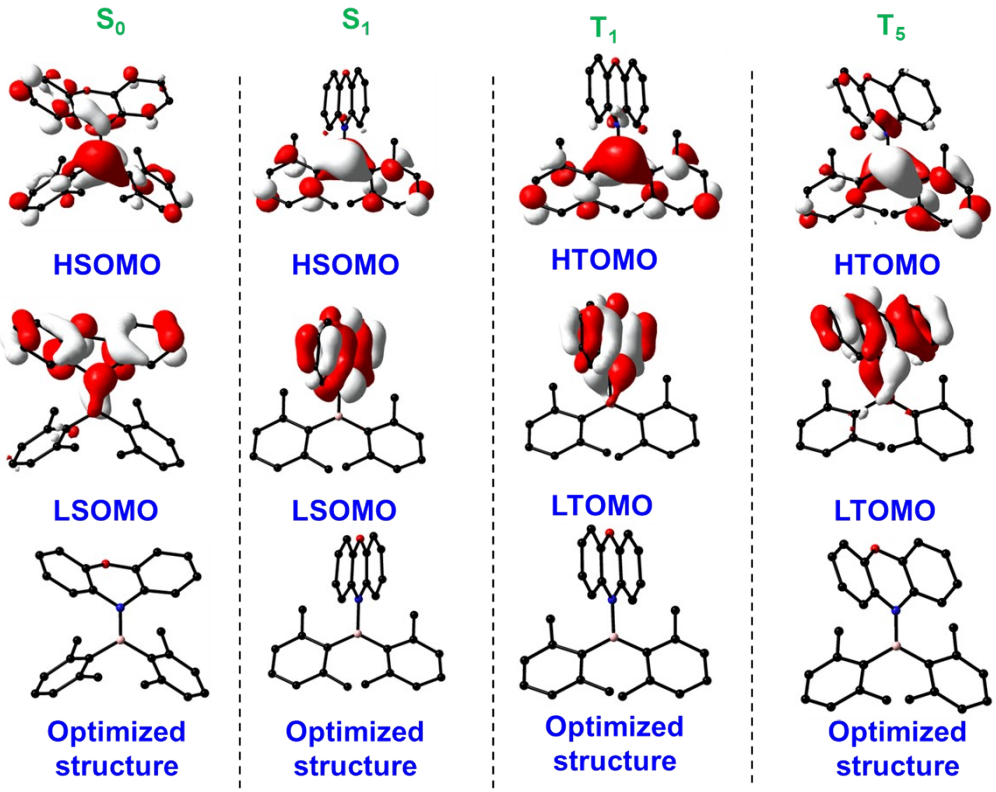

Figure S41. Optimized geometry and MOs for S_0, S_1, T_1, and T_5 for **BNO** using DFT and TD-DFT calculation with B3LYP/6-31G(d) level of theory**.** (LSOMO: Lowest occupied molecular orbital in singlet state and HSOMO: Lowest occupied molecular orbital in singlet state).

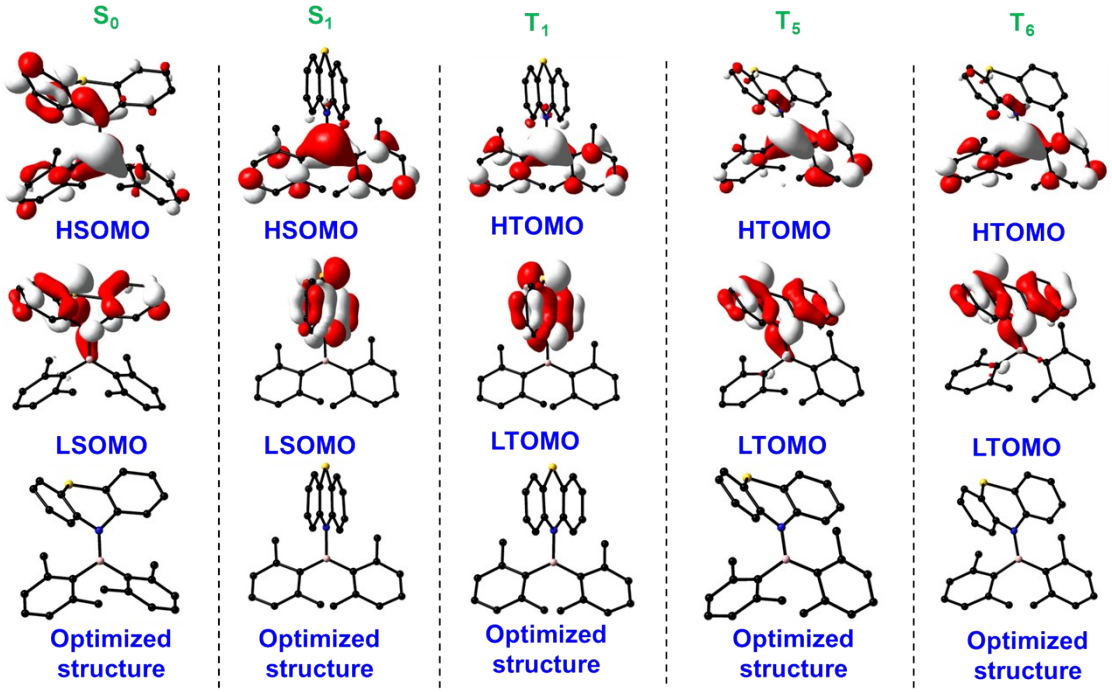

Figure S42. Optimized geometry and MOs for S_0, S_1, T_1, T_5, and T_6 for **BNS** using DFT and TD-DFT calculation with B3LYP/6-31G(d) level of theory**.** (LTOMO: Lowest occupied molecular orbital in triplet state and HTOMO: Lowest occupied molecular orbital in triplet state).

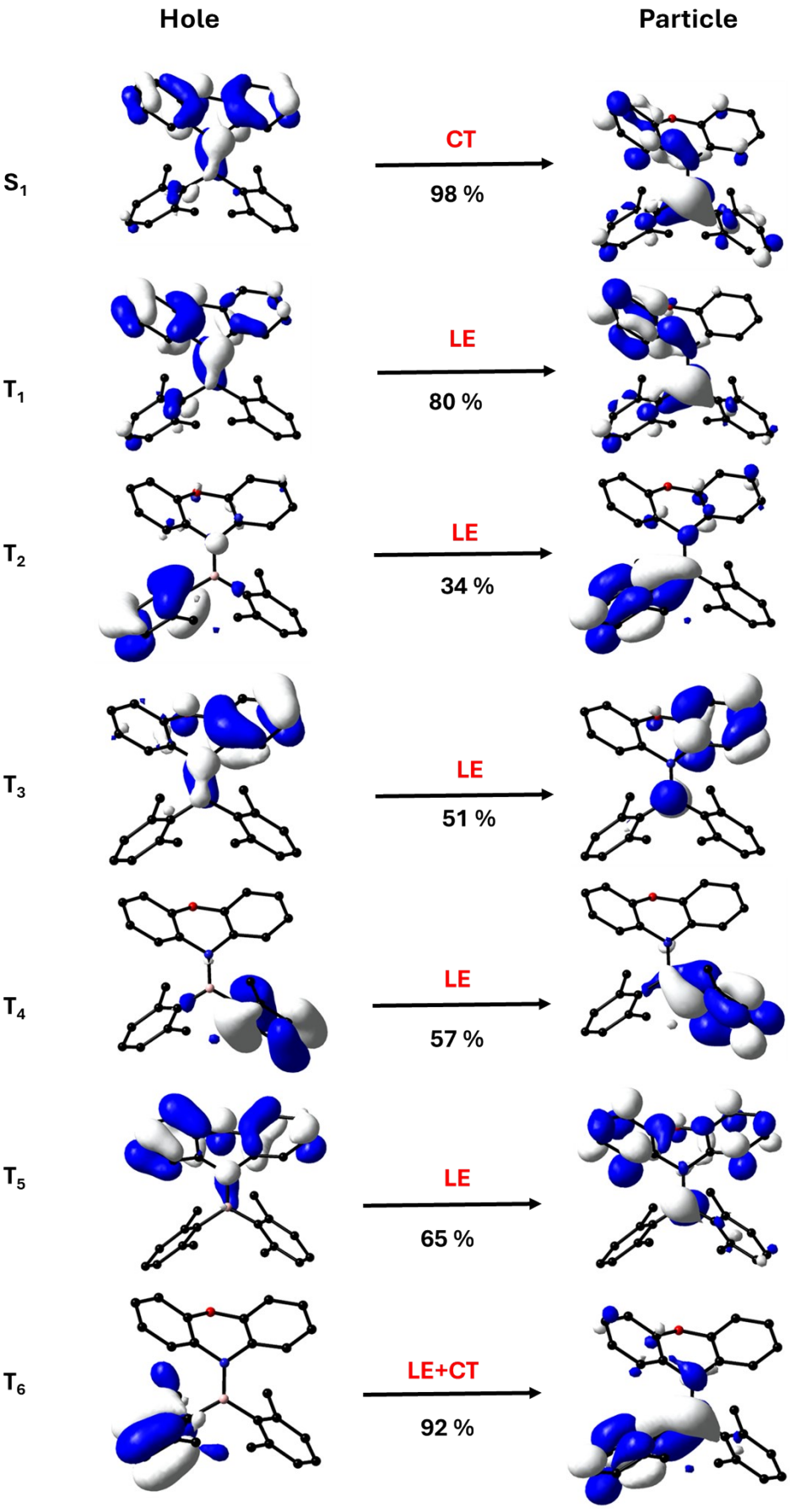

Figure S43. Natural transition orbitals (NTO) corresponding to the various states (S_1,$T_{1\text{-}6}$) of **BNO** calculated from TD-DFT calculation using B3LYP and 6-31G (d) level of theory

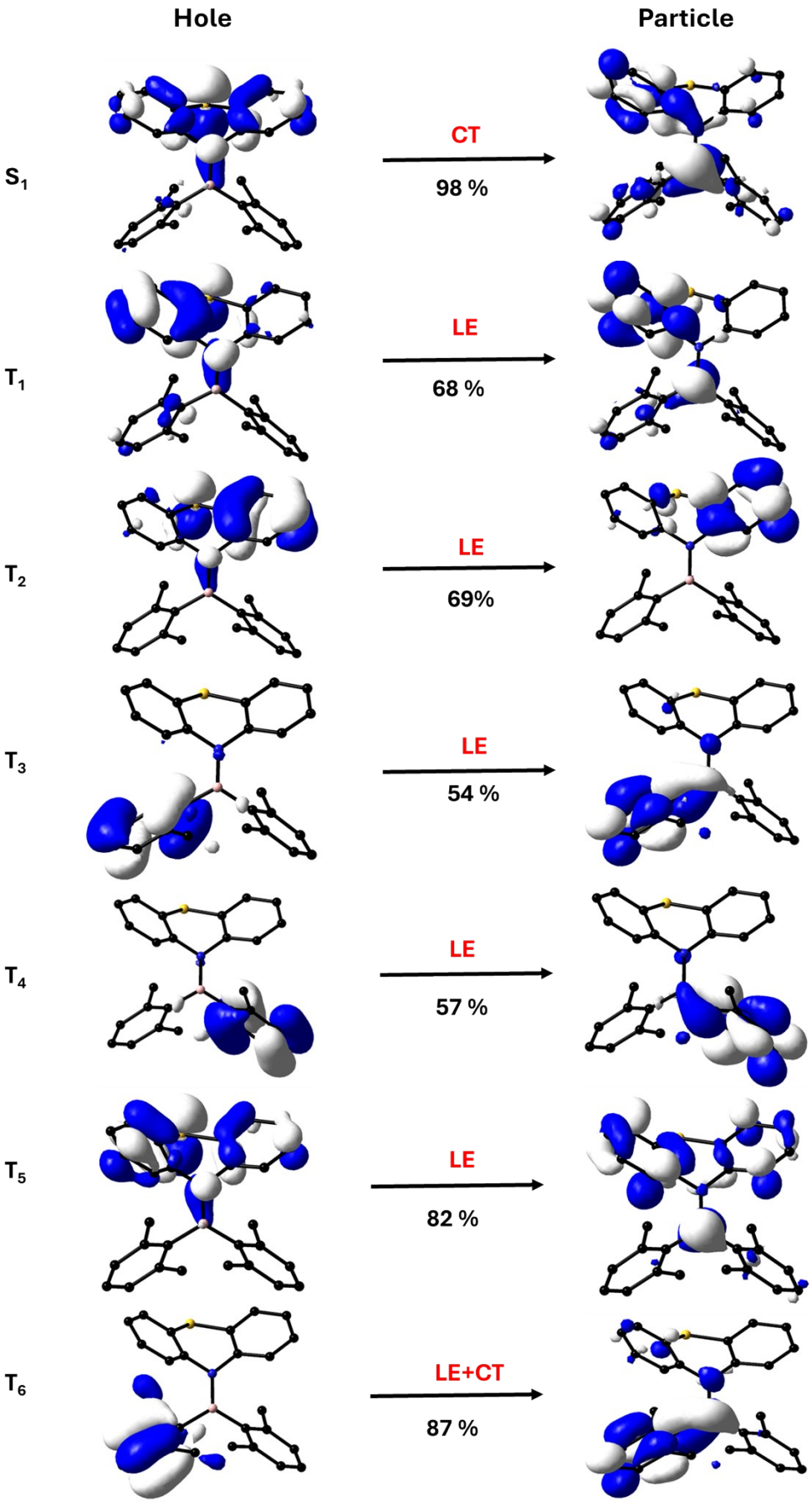

Figure S44. Natural transition orbitals (NTO) corresponding to the various states (S_1, $T_{1\text{-}6}$) of **BNS** calculated from TD-DFT calculation using B3LYP and 6-31G (d) level of theory

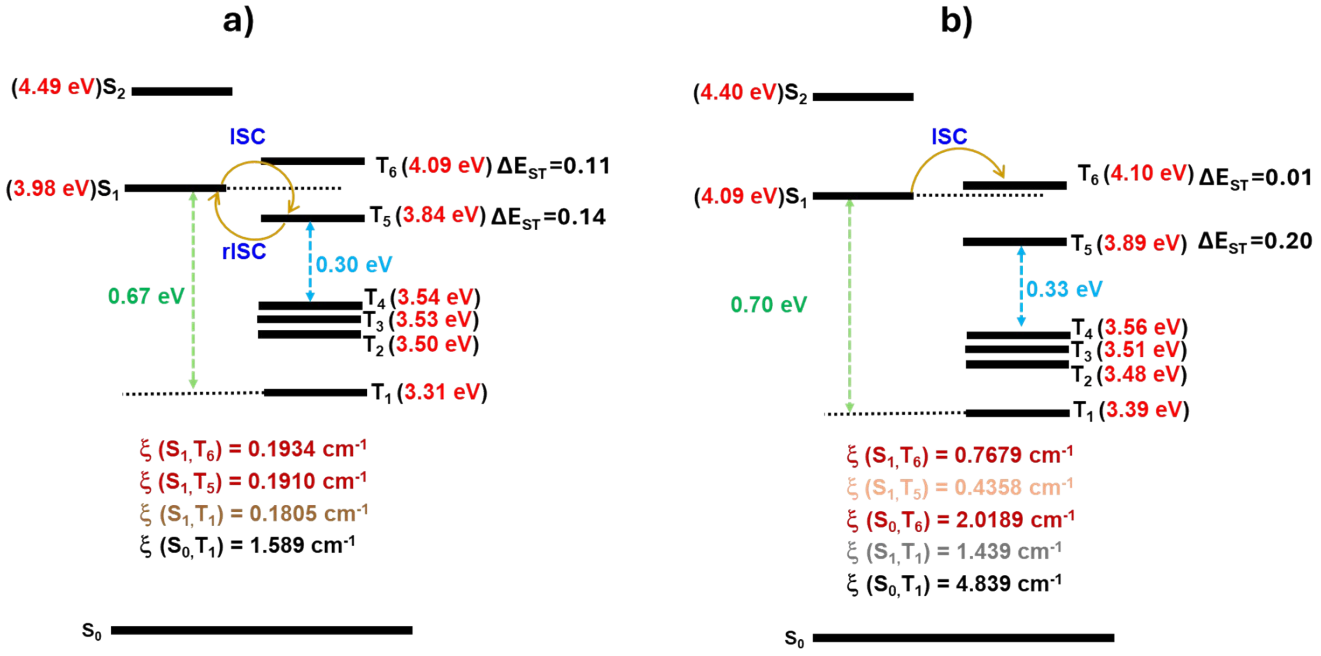

Figure S45. Energy level diagram showing singlet to triplet transitions (ISC/rISC), singlet-triplet energy gap, spin-orbital coupling constant (ξ_{SOC}), and for (a) **BNO** (b) **BNS**. Energy levels in the diagram are not up-to-scale, golden curved arrows are the most possible path according to the energy difference and spin-orbit coupling (ξ_{SOC})., ISC - intersystem crossing and rISC is reverse intersystem crossing.

Table S17. Energy onset values and singlet-triplet energy, calculated from the experimental prompt fluorescence (298K) and phosphorescence spectra at 77 K (for BNO) or 298 K (for BNS).

Compound	$^{Onset}E_S$ (Exp) [eV]	$^{Onset}E_T$ (Exp) [eV]	ΔE_{ST} (Exp) [eV]	ΔE_{S1T1} (DFT) [eV]	ΔE_{S1Tn} (DFT) [eV]
BNO (1wt%)	2.70	2.65	0.05	0.67	0.11 (T_6) 0.14 (T_5)
BNO (Solid)	2.69	2.80	0.11		
BNS (1wt%)	2.75	2.82	0.07	0.70	0.01 (T_6) 0.20 (T_5)
BNS (Solid)	3.02	2.94	0.08		

EXP= Experimentally determined, DFT- Determined vai Density functional theory

The experimental ΔE_{ST} values for BNO and BNS were determined from the spectral onset values of fluorescence spectra at 298 K ($^{onset}E_S$) and phosphorescence spectra at 77 K or 298 K ($^{onset}E_T$). The results, provided in the table below, indicate that the ΔE_{ST} values are sufficiently low to enable efficient spin crossover, resulting in significant delayed luminescence (DF/PH). Furthermore, these experimental values align more closely with the theoretically calculated ΔE_{S1Tn} values than with ΔE_{S1T1}, providing additional evidence for the involvement of higher triplet states.

Table S18. Summary of TD-DFT computed triplet vertical transitions involved in **BNO.**

Transitions	E/eV	λ/nm	f	Dominant transitions (%)	ΔE_{ST}
$S_0 \rightarrow T_1$	3.3116	374.39	0.0000	HOMO →LUMO (32.45) HOMO-2 →LUMO (2.86)	0.6662
$S_0 \rightarrow T_2$	3.5046	353.77	0.0000	HOMO →LUMO+2 (12.87) HOMO-1 →LUMO+6 (4.02)	0.4732
$S_0 \rightarrow T_3$	3.5308	351.15	0.0000	HOMO →LUMO+2 (9.23) HOMO-5 →LUMO (3.68)	0.4470
$S_0 \rightarrow T_4$	3.5404	350.19	0.0000	HOMO-4 →LUMO (7.82) HOMO-4 →LUMO+1 (6.14)	0.4374
$S_0 \rightarrow T_5$	3.8455	322.42	0.0000	HOMO →LUMO (10.82) HOMO-2 →LUMO+1 (1.59)	0.1323
$S_0 \rightarrow T_6$	4.0925	302.95	0.0000	HOMO-1 →LUMO (32.52) HOMO-1 →LUMO+1 0.(7.26)	-0.1147

Table S19. Summary of TD-DFT computed triplet vertical transitions involved in **BNS.**

Transitions	E/eV	λ/nm	f	Dominant transitions (%)	ΔE_{ST}
$S_0 \rightarrow T_1$	3.3871	366.05	0.0000	HOMO →LUMO (20.36)	0.6151
$S_0 \rightarrow T_2$	3.4762	356.67	0.0000	HOMO →LUMO+2 (24.68)	0.5821
$S_0 \rightarrow T_3$	3.5092	353.31	0.0000	HOMO-1 →LUMO+7 (8.68) HOMO-2 →LUMO+1 (5.97)	0.5306
$S_0 \rightarrow T_4$	3.5607	348.20	0.0000	HOMO-4 →LUMO+4 (9.39) HOMO-3 →LUMO+6 (6.72)	0.1988
$S_0 \rightarrow T_5$	3.8925	318.52	0.0000	HOMO →LUMO (20.17) HOMO→LUMO+1 (15.00)	-0.0138
$S_0 \rightarrow T_6$	4.1051	302.03	0.0000	HOMO-1 →LUMO (23.71)	-0.049
$S_0 \rightarrow T_6$	4.1411	299.40	0.0000	HOMO-1 →LUMO+1 (15.48)	0.7042

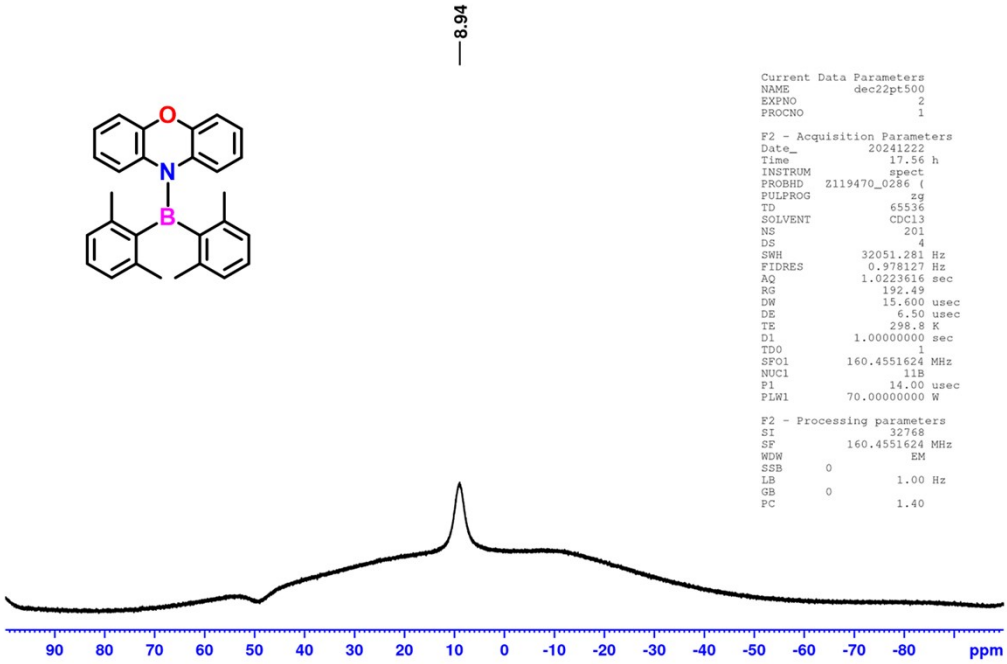

Figure S46: ^{11}B NMR of **BNO** in $CDCl_3$ at 25°C after adding an excess tetrabutylammonium fluoride TBAF. (^{11}B NMR before adding TBAF is in S3).

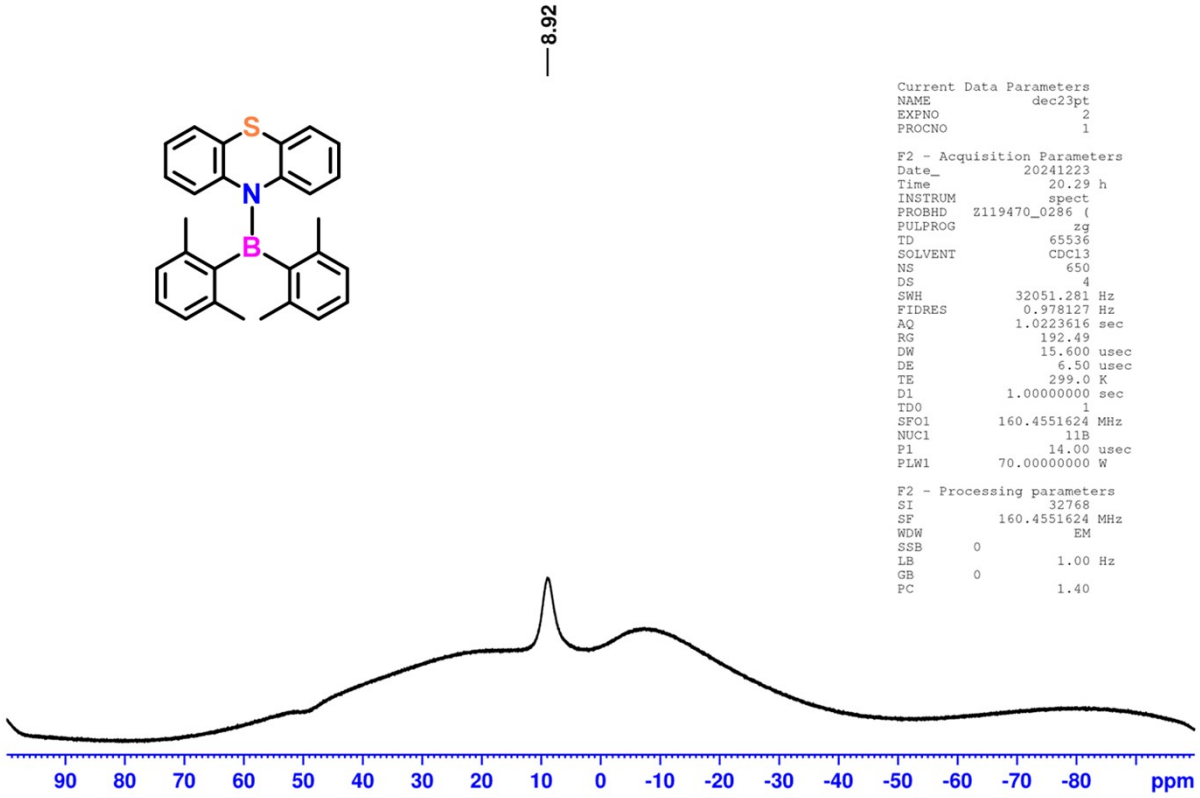

Figure S47: ^{11}B NMR of **BNS** in $CDCl_3$ at 25°C after adding an excess tetrabutylammonium fluoride (TBAF). ^{11}B NMR before adding TBAF is in S7.

Table S20. Coordinates of **BNO** after single-point energy calculations.

Center Number	Atomic Number	Atomic Type	Coordinates (Angstroms) X	Y	Z
1	6	0	-2.453196	-0.023394	-2.330780
2	1	0	-1.559222	0.324536	-2.286001
3	1	0	-2.481473	-0.753517	-2.952887
4	1	0	-3.051260	0.668978	-2.621989
5	8	0	3.081225	-1.275978	-0.771115
6	6	0	-0.336147	4.486402	-1.105579
7	1	0	-0.271577	5.381309	-1.349760
8	6	0	-1.050591	4.122204	0.008357
9	1	0	-1.469838	4.779220	0.516100
10	6	0	-1.160750	2.788718	0.392658
11	6	0	-0.480073	1.789582	-0.332181
12	5	0	-0.588912	0.246870	0.035057
13	7	0	0.622506	-0.485114	0.259319
14	6	0	1.827341	0.173882	0.659404
15	6	0	1.834659	1.180224	1.616296
16	1	0	1.035206	1.448596	2.008189
17	6	0	3.019783	1.787687	1.992502
18	1	0	3.010805	2.469183	2.625277
19	6	0	4.212068	1.386361	1.433028
20	1	0	5.004603	1.805903	1.679603
21	6	0	-4.578287	-1.530004	0.390434
22	1	0	-5.430821	-1.891804	0.472141
23	6	0	-3.750510	-1.471870	1.479120
24	1	0	-4.051999	-1.787540	2.300384
25	6	0	-2.463510	-0.947640	1.376767
26	6	0	-1.607815	-0.944752	2.615621
27	1	0	-0.751612	-0.560359	2.412206
28	1	0	-2.036770	-0.426189	3.299956
29	1	0	-1.488284	-1.845947	2.924236
30	6	0	-2.006509	-0.450773	0.133348
31	6	0	-4.144455	-1.050950	-0.824379
32	1	0	-4.712076	-1.091503	-1.559916
33	6	0	0.280095	3.522602	-1.852698
34	1	0	0.728638	3.768715	-2.629350
35	6	0	0.253281	2.176205	-1.478999
36	6	0	1.006304	1.201435	-2.344303
37	1	0	0.911825	0.315891	-1.985695
38	1	0	0.651719	1.224915	-3.236129
39	1	0	1.935546	1.441618	-2.363040
40	6	0	-2.003083	2.460002	1.589730
41	1	0	-1.990043	1.511572	1.739404
42	1	0	-1.652580	2.910512	2.361371
43	1	0	-2.906009	2.746603	1.434117
44	6	0	4.233918	0.364678	0.508767
45	1	0	5.039426	0.083586	0.138465
46	6	0	3.044484	-0.239826	0.136423
47	6	0	2.086829	-2.219732	-0.589458
48	6	0	2.377416	-3.518497	-0.971072
49	1	0	3.206158	-3.724464	-1.339316

50	6	0	1.430888	-4.501415	-0.801356
51	1	0	1.618315	-5.376160	-1.055675
52	6	0	0.205846	-4.191027	-0.255122
53	1	0	-0.429855	-4.859910	-0.139119
54	6	0	-0.088762	-2.889111	0.123806
55	1	0	-0.918113	-2.694014	0.496541
56	6	0	0.847128	-1.871812	-0.049173
57	6	0	-2.870268	-0.505920	-0.972944

Table S21. Coordinates of **BNS** after single-point energy calculations.

Center Number	Atomic Number	Atomic Type	Coordinates (Angstroms) X	Y	Z
1	16	0	-3.210747	-0.857667	1.156020
2	6	0	-0.952581	-1.794514	-0.099507
3	6	0	2.734031	-0.864579	1.175439
4	7	0	-0.590139	-0.406875	-0.288959
5	6	0	-0.163843	-2.838183	-0.572919
6	1	0	0.625737	-2.653801	-1.025871
7	6	0	0.754958	1.772705	0.281587
8	6	0	-2.940277	0.313222	-0.131392
9	6	0	-1.514315	1.315689	-1.751281
10	1	0	-0.689603	1.360280	-2.179082
11	6	0	-1.690162	0.420673	-0.697611
12	6	0	2.026249	-0.669263	-0.026876
13	6	0	3.835010	-1.790279	-1.194330
14	1	0	4.213027	-2.088616	-1.991458
15	6	0	0.996530	4.484879	0.970648
16	1	0	1.074236	5.381394	1.199426
17	6	0	2.598181	-1.149640	-1.211402
18	6	0	2.175572	-0.403116	2.496804
19	1	0	2.132160	0.556519	2.508285
20	1	0	2.746587	-0.704532	3.208053
21	1	0	1.294040	-0.766115	2.616536
22	6	0	1.514009	2.662883	-0.513882
23	5	0	0.694626	0.202192	-0.031956
24	6	0	0.131301	2.295408	1.413130
25	6	0	-2.535010	2.131812	-2.169338
26	1	0	-2.395555	2.747058	-2.853327
27	6	0	-1.736577	-4.448607	0.244343
28	1	0	-1.999655	-5.334244	0.361776
29	6	0	-3.983854	1.119514	-0.574609
30	1	0	-4.828440	1.035864	-0.197361
31	6	0	1.611771	4.012193	-0.149429
32	1	0	2.102499	4.594141	-0.680247
33	6	0	-2.138832	-2.103203	0.538366
34	6	0	3.958451	-1.522683	1.178864
35	1	0	4.415822	-1.650947	1.978370
36	6	0	4.500621	-1.985318	-0.009661
37	1	0	5.318523	-2.426607	-0.007293
38	6	0	0.277021	3.654934	1.745992
39	1	0	-0.131424	3.985131	2.514236

40	6	0	1.923155	-1.044338	-2.563456
41	1	0	1.054201	-0.651913	-2.456351
42	1	0	1.833181	-1.920848	-2.947008
43	1	0	2.454304	-0.494886	-3.143264
44	6	0	-2.532989	-3.432004	0.690510
45	1	0	-3.346170	-3.628636	1.098400
46	6	0	-3.769156	2.031806	-1.564919
47	1	0	-4.462011	2.589258	-1.835305
48	6	0	-0.558981	-4.163414	-0.370855
49	1	0	-0.011427	-4.856635	-0.659306
50	6	0	-0.721535	1.473730	2.363407
51	1	0	-1.647677	1.692176	2.231015
52	1	0	-0.471951	1.671864	3.270946
53	1	0	-0.584930	0.539959	2.189582
54	6	0	2.231431	2.221075	-1.745366
55	1	0	2.842331	1.516048	-1.524028
56	1	0	2.716239	2.959536	-2.117464
57	1	0	1.594689	1.900090	-2.386628

---

6. References

[1] M. J. Frisch, G. W. Trucks, H. B. Schlegel, G. E. Scuseria, M. A. Robb, J. R. Cheeseman, G. Scalmani, V. Barone, G. A. Petersson, H. Nakatsuji, X. Li, M. Caricato, A. V. Marenich, J. Bloino, B. G. Janesko, R. Gomperts, B. Mennucci, H. P. Hratchian, J. V. Ortiz, A. F. Izmaylov, J. L. Sonnenberg, Williams, F. Ding, F. Lipparini, F. Egidi, J. Goings, B. Peng, A. Petrone, T. Henderson, D. Ranasinghe, V. G. Zakrzewski, J. Gao, N. Rega, G. Zheng, W. Liang, M. Hada, M. Ehara, K. Toyota, R. Fukuda, J. Hasegawa, M. Ishida, T. Nakajima, Y. Honda, O. Kitao, H. Nakai, T. Vreven, K. Throssell, J. A. Montgomery Jr., J. E. Peralta, F. Ogliaro, M. J. Bearpark, J. J. Heyd, E. N. Brothers, K. N. Kudin, V. N. Staroverov, T. A. Keith, R. Kobayashi, J. Normand, K. Raghavachari, A. P. Rendell, J. C. Burant, S. S. Iyengar, J. Tomasi, M. Cossi, J. M. Millam, M. Klene, C. Adamo, R. Cammi, J. W. Ochterski, R. L. Martin, K. Morokuma, O. Farkas, J. B. Foresman, D. J. Fox, Wallingford, CT, 2016.

[2] T. A. K. Roy Dennington, and John M. Millam, Semichem Inc., Shawnee Mission, KS, 2016

[3] (a) D. G. Chen, T. C. Lin, C. L. Chen, Y. T. Chen, Y. A. Chen, G. H. Lee, P. T. Chou, C. W. Liao, P. C. Chiu, C. H. Chang, Y. J. Lien and Y. Chi, ACS Appl Mater Interfaces, 2018, 10, 12886–12896.(b)K. K. Neena, P. Sudhakar, K. Dipak and P. Thilagar, *Chemical Communications*, 2017, **53**, 3641–3644

[4] (a) C. A. Swami and P. Thilagar, *Inorg Chem*, 2014, **53**, 2776–2786.(b) S. K. Sarkar, S. E. Rao and P. Thilagar, *J Phys Chem B*, 2020, **124**, 8896–8903.(c) P. Thilagar, R.P. Nandi, S.Ghosh , *Chem. Eur. J.* 2024, **30**, e202400398

[5] (a) K. Goushi, K. Yoshida, K. Sato, C. Adachi, *Nat Photonics* 2012, ***6***, 253–258 (b) K. Masui, H. Nakanotani, C. Adachi, *Org Electron* 2013, ***14***, 2721–2726.(c) T. Nakagawa, S. Y. Ku, K. T. Wong, C. Adachi, *Chemical Communications* 2012, ***48***, 9580–9582. (d) G. Méhes, H. Nomura, Q. Zhang, T. Nakagawa, C. Adachi, *Angewandte Chemie - International Edition* 2012, ***51***, 11311–11315. (e) N. Notsuka, H. Nakanotani, H. Noda, K. Goushi, C. Adachi, *Journal of Physical Chemistry Letters* 2020, ***11***, 562–566.